PUBLISHED BY INSTITUTE OF PHYSICS PUBLISHING AND SISSA
RECEIVED: *November 29, 2007*
ACCEPTED: *January 14, 2008*
PUBLISHED: *February 21, 2008*

The ATLAS Forward Calorimeters

A. Artamonov,[a] D. Bailey,[b] G. Belanger,[c1] M. Cadabeschi,[b] T.-Y. Chen,[d] V. Epshteyn,[a] P. Gorbounov,[b2] K.K. Joo,[b3] M. Khakzad,[c4] V. Khovanskiy,[a] P. Krieger,[b] P. Loch,[e] J. Mayer,[b5] E. Neuheimer,[c†] F.G. Oakham,[c6] M. O'Neill,[c7] R.S. Orr,[b] M. Qi,[d] J. Rutherfoord,[e*] A. Savine,[e] M. Schram,[c] P. Shatalov,[a] L. Shaver,[e†] M. Shupe,[e] G. Stairs,[b8] V. Strickland,[c6] D. Tompkins,[e] I. Tsukerman[a] and K.Vincent[b]

[a] *Institute of Theoretical and Experimental Physics, RU-117259 Moscow, Russia*
[b] *University of Toronto, ON M5S 1A7, Canada*
[c] *Carleton University, Ottawa, ON K1S 5B6, Canada*
[d] *Nanjing University, Nanjing 210093, China*
[e] *University of Arizona, Tucson, AZ 85721, U.S.A.*
[1] *Now at European Space Agency, Madrid*
[2] *Permanent Address ITEP, Moscow*
[3] *Now at Chonnam National University, Chonnam, Republic of Korea*
[4] *Now at Dept. of Physics, St. Francis Xavier University, Antigonish, NS, B2G 2W5, Canada*
[5] *Now at Apotex, Canada, Inc.*
[6] *Also at TRIUMF, Vancouver, B.C. V6T 2A3, Canada*
[7] *Now at BeconRidge, Ottawa, Ontario, Canada*
[8] *Now in the private sector*
E-mail: rutherfo@physics.arizona.edu

ABSTRACT: Forward calorimeters, located near the incident beams, complete the nearly 4π coverage for high p_T particles resulting from proton-proton collisions in the ATLAS detector at the Large Hadron Collider at CERN. Both the technology and the deployment of the forward calorimeters in ATLAS are novel. The liquid argon rod/tube electrode structure for the forward calorimeters was invented specifically for applications in high rate environments. The placement of the forward calorimeters adjacent to the other calorimeters relatively close to the interaction point provides several advantages including nearly seamless calorimetry and natural shielding for the muon system. The forward calorimeter performance requirements are driven by events with missing E_T and tagging jets.

KEYWORDS: Calorimeters; Large detector systems for particle and astroparticle physics.

* Corresponding author.
† Retired.

2008 JINST 3 P02010

Contents

1. Introduction **1**

2. Performance requirements **2**

3. The Forward Calorimeters as a part of the ATLAS detector **3**

4. The FCal mechanical design **4**

4.1 The liquid argon technology 4

4.2 The electrodes 5

4.3 The FCal modules 8

4.4 The unit cell 11

4.5 The FCal1 module 13

4.6 The FCal2 and FCal3 modules 15

5. The electrical signal **20**

6. Noise **26**

7. Segmentation **26**

8. HV distribution **28**

9. Final assembly **28**

10. Integration of the FCals into the cryostats **32**

11. Test beam performance **34**

12. QA/QC **35**

13. Materials certification **36**

14. Summary **36**

1. Introduction

The Large Hadron Collider (LHC) at the CERN laboratory will collide 7 TeV protons against 7 TeV protons. Because the cross sections of interest are small, the LHC will operate at a luminosity of $\mathcal{L} = 10^{34}$ cm^{-2} s^{-1}. The exceptionally high luminosity presented a particular challenge in the design of the two LHC detectors that focus on "high p_T physics". The plentiful ordinary "low p_T" or "soft" minimum-bias (min-bias) collisions will illuminate all the detector elements with background particles, leading to several problems. For the liquid argon

2008 JINST 3 P02010

calorimeters in the ATLAS detector, and particularly for the forward calorimeters (FCal) near the beam directions, there will be a nearly constant bombardment of particles creating a low level of ionization in the electrode gaps at every bunch crossing.

At a high luminosity hadron collider such as the LHC the min-bias particle densities and energies are largest at high $|\eta|$, i.e. near the forward and backward directions. Calorimetry is the only useful detector technology which survives in this harsh environment. Many calorimeter design compromises are imposed to meet the stringent requirements.

In the ATLAS detector at the LHC [1] the inner tracker coverage extends up to $|\eta|=2.5$, the muon coverage up to $|\eta|=2.7$, and the precision calorimetry for electrons and gammas up to $|\eta|=2.5$. Beyond this, the only coverage is calorimetric and extends to $|\eta|=4.9$. In this region ATLAS focuses on jets. The ATLAS forward calorimeters cover the region $3.1 < |\eta| < 4.9$.

A major objective of forward calorimetry is physics with missing E_T. High p_T neutrinos and other weakly interacting particles will escape detection but their presence can be inferred by observing events with large momentum imbalance in the direction transverse to the beams. Backgrounds come from ordinary events where a jet escapes detection, often down the beam hole, or where the jet is badly mismeasured. Forward calorimeters close as much of this beam hole as is practical, thereby completing the nearly hermetic calorimeter system. And a quality calorimeter minimizes the occasional poor energy measurement.

Benchmark physics processes which have guided our performance goals include Standard Model intermediate-mass Higgs production with subsequent decay to real or virtual Z pairs with one Z decaying to charged leptons (electrons or muons) and the other decaying to unobserved neutrinos. The on-going search for Supersymmetry (SUSY) will have pushed the gluino mass limit to 300 GeV at LHC turn-on ([2], page 84) so missing E_T greater than 100 GeV will set the scale. Observation of these generic processes requires small non-Gaussian tails on the E_T resolution function. The process $A/H \rightarrow \tau^+\tau^-$ requires good E_T resolution and is not sensitive to the tails. Longitudinal WW, WZ, and ZZ scattering (Vector Boson fusion) processes leave two recoil jets near the forward and backward directions which can be used as tags to enhance the signal over background. Many of these tagging jets will fall in the forward calorimeters and it will be a challenge to pick these out above the pileup noise. Physics processes of this kind place different requirements on the Forward Calorimeter, all of which we have tried to meet.

2. Performance requirements

To minimize instrumental contributions to the missing E_T signal we require hermetic calorimetry with good energy and position resolution and with small tails on the resolution function. The non-Gaussian tails on the energy resolution function must be small so that instrumental contributions to the missing E_T signal are negligible compared to the expected physics signals.

The forward calorimeters detect jets, in particular tagging jets or jets which would otherwise escape detection and lead to false missing E_T signatures. This sets the segmentation of the readout to be of order $\Delta\eta \times \Delta\varphi = 0.1 \times 0.1$ in the front and 0.2×0.2 at the back.

We set the E_T resolution requirement to be $\Delta E_T/E_T < 10\%$ for $E_T > 25$ GeV. Below $E_T \approx 25$ GeV, tagging jets are lost in the pileup. This requires an FCal energy resolution of typically $\Delta E/E < 7\%$ and a jet angular resolution of $\Delta\theta/\theta < 7\%$ for energies above 250 GeV. At the highest $|\eta|$ it is the angular resolution which dominates.

Physics pileup in the FCal measured in terms of E_T is about the same as at central $|\eta|$. In order to minimize this pileup, a fast response is required, of order a beam crossing interval of 25 ns.

2008 JINST 3 P02010

The dynamic range of the readout channels is set at the low end by the electronics noise. Because the electronics noise is well understood and is consistent from one channel to the next we set the gain so that the noise level is about 5 ADC counts rms, allowing a measurement of comparable precision to the prediction. At the high end the gain must accommodate an energy in a single channel of about half the kinematic limit of 7 TeV.

The forward calorimeters must be especially radiation hard to ensure long-term stability when the LHC is running at its design luminosity of $\mathcal{L} = 10^{34}$ cm^{-2} s^{-1}. To set the scale, at every 25 ns beam crossing, roughly 7 TeV of energy is deposited in each of the two FCals [3]. This corresponds to a power of approximately 45 Watts. The ionization dose varies throughout the FCal from a low of about 10 kRad to values approaching 0.5 GRad per LHC year. The flux of neutrons with kinetic energies above 100 keV ranges from 10^4 to 10^6 kHz/cm^2.

3. The Forward Calorimeters as a part of the ATLAS detector

The severe environment near the beam line, dominated by products of collisions at the interaction point (IP), suggests locating the forward calorimeters as far from the IP as possible. This reduces the particle densities and therefore the radiation damage. The original ATLAS design [4] placed the FCal at about 15 m from the IP. But further study [5]-[8] showed there were many advantages to locating the FCal at roughly the same distance as the endcap calorimeters, i.e. *integrated* into the endcap (figure 1)[1]. The distance of the ATLAS FCal from the IP is now about 5 m where the density of particles is approximately 9 times greater. Despite the high background rates there are many advantages to this design strategy [9].

The calorimetry system is now manifestly *hermetic*. A deep calorimeter system continuously surrounds the IP (with non-projective gaps to route signals and services for the inner tracker). A key feature is that un-instrumented *transitions* from one calorimeter system to another are minimized. Transitions can be problematic in that hadronic showers near the edges can be absorbed in structural material or can spray into remote calorimeters with no hint that the energy did not come directly from the IP. This leads to false reconstruction of the energy flow. The endcap-forward transition in ATLAS now suffers little of this effect [6],[10].

ATLAS has an *open* muon system, i.e. the muon chambers are not embedded between magnetized iron slabs which would provide natural shielding. So the ATLAS muon chambers are fully exposed to backgrounds (particularly neutrals) in the collision hall. In the early, far forward FCal design, ATLAS had deployed massive shielding in order to reduce these backgrounds to manageable levels. The newer *integrated* design allows more flexibility in optimizing the muon shielding [11],[12] yielding important reductions in the background rates.

With a far forward calorimeter, ATLAS was required to leave a clear space from the IP to the FCal so as not to obstruct the particles. This clear space, the need to deploy massive shielding close to the beamline, the desire for muon coverage at high values of $|\eta|$, and the beam line appurtenances were all in conflict. The space was oversubscribed. The *integrated* design ameliorated these conflicts.

There is unavoidable material upstream of all the ATLAS calorimeters. This material is particularly troublesome near the beam line in front of the FCal. Examples include the beam pipe itself which is crossed at shallow angles by the particles, but, in addition, includes flanges, valves, vacuum pumps, vacuum bake-out appliances, support structures, inner tracker supports

[1] Figure kindly provided by Roy Langstaff at University of Victoria and TRIUMF.

2008 JINST 3 P02010

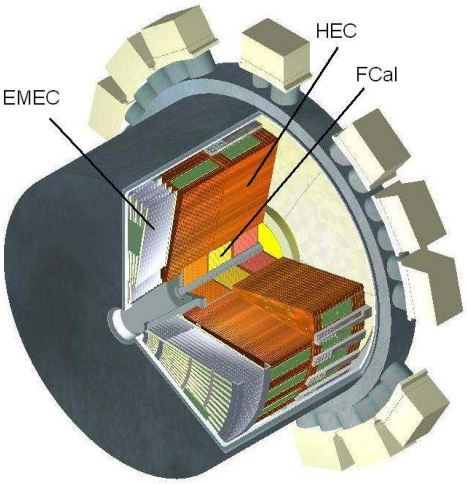

Figure 1. Cut-away drawing of one EndCap Cryostat with the interaction point off to the lower left. The calorimeters in this cryostat are the endcap calorimeters (the EMEC and HEC), and the FCal.

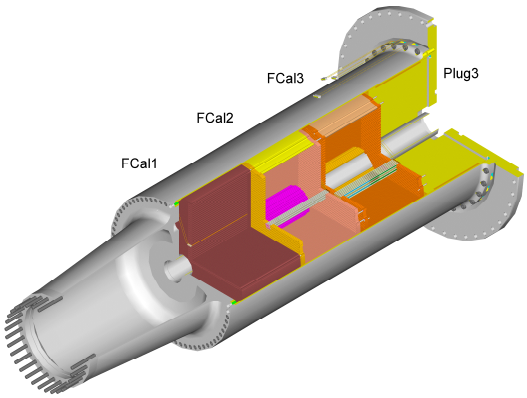

Figure 2. The three FCal modules and "Plug3" sit within the support tube, a structural member of the cryostat.

and services, and, in the case of ATLAS, cryostat walls. With the *integrated* FCal there is less of this material but, also important, the *lever arm* from the material to the FCal is much smaller. For particles which shower in the upstream material, that shower cannot spread much over the short distance to the FCal so the energy flow is well collimated along the original direction. For a far forward calorimeter, on the other hand, the far upstream material causes the energy to spread over such a large area of the FCal that much of it is lost in the pileup.

The *integrated* FCal is denser than the neighboring calorimeters. It has the same depth measured in interaction lengths but is physically shorter allowing the front face to be set back from the front face of the neighboring calorimeters. The resulting alcove upstream of the FCal is lined with boron-loaded polyethylene to reduce neutron albedo into the tracker volume to acceptable levels.

Finally, the smaller physical size of the *integrated* FCal leads to financial savings, some of which can be used for a higher quality device.

4. The FCal mechanical design

4.1 The liquid argon technology

The FCal is a liquid argon, ionization, sampling calorimeter [13]. Because liquid argon and the absorber metals are radiation hard it is anticipated that the FCal performance will be stable over the life of the detector. Care was required in selecting the several additional materials (e.g. readout cables) which go into the construction in order to ensure they also will not degrade with the expected radiation exposure. The choice of liquid argon is natural because the FCal lies within the ATLAS Hadronic Endcap Calorimeter (HEC) [14] which is a liquid argon parallel plate design. Along with the EM endcap 'Spanish Fan' (EMEC), the HEC and FCal all sit within the same cryostat as can be seen in figure 1.

The modules making up the FCal and the shielding plug are held within a cryostat structural member (support tube) as shown in figure 2. The function of this support tube is primarily to hold the inner cold vessel of the cryostat together against pressures up to 3 atmospheres with vacuum between it and the warm vessel. More information on the support tube is provided in sections 9 and 10.

2008 JINST 3 P02010

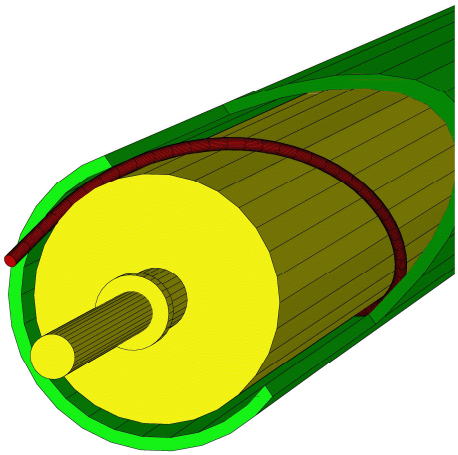

Figure 3. Cut-away drawing of an FCal electrode. Liquid argon fills the gap between the rod and tube.

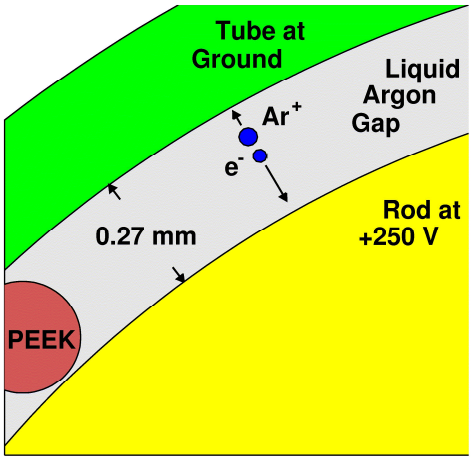

Figure 4. Close-up view of a cross-section of the FCal1 electrode gap. The insulating PEEK fiber is shown.

4.2 The electrodes

The ATLAS FCal is not a conventional liquid argon calorimeter. The liquid argon gap in the FCal1 module is chosen to be roughly an eighth of the usual 2 mm gap to avoid the ion buildup problem [15] resulting from the low mobility of the positive charge carriers in the argon. At sufficiently high ionization rates (due to the copious min-bias events) a threshold is reached above which the charge accumulation distorts the electric field sufficiently to degrade the signal from the drifting electrons. Smaller gaps allow the FCal to stay below this threshold at the LHC design luminosity. The smaller gaps also lead to a much faster signal. The triangular current pulse at the electrode has a full drift time of about 61 ns in FCal1 as opposed to the 450 ns of more conventional 2 mm gaps in many liquid argon sampling calorimeters. After 25 ns, 66% of the signal has already accumulated on the electrode. The reader will note that we are using the term “electrode” to refer to the anode (rod), the cathode (tube), and the liquid argon ionization medium in the gap between the concentric rod and tube.

The liquid argon gap in the FCal2 module is about 50% larger than in FCal1 while that in the FCal3 is about twice that in FCal1. These larger gaps deeper in the calorimeter are acceptable because the ionization density from showers is lower than in the FCal1 module. The nearest-neighbor spacing of electrodes in the FCal1 module is 7.5 mm center-to-center and increases in the FCal2 and FCal3 modules so that they are pseudo-projective. The radius of the cylindrical shell liquid argon gap was chosen to be a third of the nearest-neighbor spacing to optimize the sampling uniformity [16].

Precision small gaps are difficult to maintain in a parallel plate design so the electrode structure was chosen based on tubes and rods as shown in figure 3 and figure 4. The gap between the inner solid rod and the outer tube is maintained by a helically-wound PEEK fiber whose diameter is slightly smaller than the gap. Liquid argon, the ionizing (sensitive) medium, fills the rest of the gap not occupied by the fiber (98.8% of the volume of the gap for FCal1). The rod is held at positive potential and the tube at ground. The current of electrons drifting toward the rod constitutes the signal [17]. The rod is made of the same material as the absorber matrix. The electrodes form an hexagonal array as shown in figure 5.

2008 JINST 3 P02010

Figure 5. Photo of the front face of the FCal1 module during construction. The beam hole is partially visible in the upper right.

	FCal1	FCal2C	FCal2A	FCal3
Tube Length	445.0N	444.35N	444.35N	444.3
Tube OD	5.753	6.185	6.165	7.01
Tube Wall Thickness	0.252	0.258	0.234	0.250N
Tube ID	5.250	5.669	5.697	6.51
Rod Length	445.2	443.48	443.48	443.4
Rod OD	4.712	4.93	4.93	5.495
Gap (calc)	0.269	0.369	0.383	0.508
PEEK fiber OD	0.250N	0.350N	0.350N	0.467
PEEK fiber windings	~12	~8	~8	~8

Table 1. Physical dimensions of the electrode components at room temperature. Units are mm. N means "nominal", i.e. no measurement was made. The Gap is calculated as half the difference of the Tube inner diameter (ID) and the Rod outer diameter (OD).

The axis of each electrode is parallel to the nominal beam line of the LHC so that particles from the interactions impinge on the calorimeter at a shallow angle to the electrode axis. In order that the size of the electrical signal from the Forward Calorimeter be insensitive to the position of the particle, it is important that the electrodes in a module be as identical as possible. The dimensions of the electrode components are summarized in table 1. The liquid argon "Gap" is the critical parameter for the electrical signal. Detailed metrology for FCal1 electrode elements predicted the rms gap width variation to be about 1%. Similar results were obtained for FCal2 and FCal3.

2008 JINST 3 P02010

	Calculated Capacitance	Measured Capacitance
FCal1C Electrodes	234.4	235.8(1.8)
FCal1A Electrodes	234.4	236.4(1.8)
FCal2C Electrodes	182.4	179.5(2.4)
FCal2A Electrodes	175.5	174.8(3.0)
FCal3C Electrodes	152.0	149.2(1.8)
FCal3A Electrodes	152.0	150.8(1.7)

Table 2. Summary of calculated and measured FCal electrode capacitances in room temperature air. Units are picofarads. Numbers in parentheses are rms spread in measurements.

From the data in table 1, the capacitance of these electrodes can be estimated by hand but to account for the PEEK fiber and end effects, an FEA electric field analysis was used to give the results shown in table 2.

To confirm the calculated capacitance and rms variation, measurements of the electrode capacitance for every electrode in every module were performed [18]. This was done in a clean room so the dielectric of the gap was standard air at about 380 m altitude and about 40% relative humidity rather than liquid argon. A summary of the results is shown in table 2.

The rms of the capacitance measurements for FCal1 is about 0.8%, consistent with the metrology noted above. For FCal2 the rms is about 1.5% and for FCal3 about 1.2%. This data suggests that the variation of the gap width of the electrodes is significantly smaller than the constant term in the energy resolution. Capacitance measurements of the one reference electrode, measured periodically to check for drift, had an rms of about 0.15% after rejection of a few outliers. The rms capacitance measurement of a 400 pF standard capacitor was about 0.02% (about 0.1 pF). So drift or other instrumental effects are likely a small contribution to the measured electrode rms values.

The measured signal for a particle showering in the calorimeter depends on the sampling fraction of the calorimeter. This sampling fraction depends on the dimensions of the gap and the dimensions of the gap vary by a small amount from electrode to electrode. The capacitance measurements provide a measure of this variation, averaged over the length of the electrode. If our electronics integrated the charge deposited in the gap, then the rms of the capacitance measurements would provide an estimate of the rms spread of gains. In the other extreme, if the electronics provided very fast shaping then the measurement would be proportional to the initial current on the pulse. The initial current depends on the product of the charge density and the electron drift velocity. The drift velocity depends on the electric field in the gap. Since all electrodes in a given FCal module are held at the same potential, this electric field varies from electrode to electrode depending on the gap giving a smaller initial current and therefore a smaller signal for a larger gap. The electronics in ATLAS is at neither of these extremes. Detailed calculations show the fractional variation in the signal is smaller than the fractional variation in the dimensions of the gap [19].

The electrode tubes are held in the calorimeter end-plates by swaging (expanding the tube at one position along its length) into a groove in the electrode hole in the matrix as shown in figure 6. At the readout end, the groove has a sharp feature which cuts into the copper tube, making a positive electrical contact. The short expanded section of the tube gives a larger gap at this position which we neglect in any calculations.

2008 JINST 3 P02010

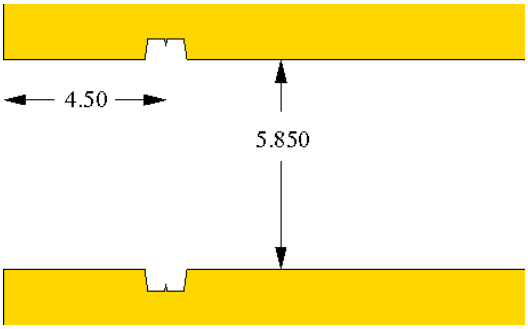

Figure 6. Cross section of one end of the electrode hole in an FCal1 module end plate showing the swage groove with the sharp feature which cuts into the copper tube outer surface when the tube is swaged. The swage groove and sharp feature are shown 4 times actual depth for clarity. Units are mm.

In the ATLAS accordion and HEC calorimeters, the functions of protection resistors and blocking capacitors are integrated into the electrode structures via resistive coatings and layered electrodes. In order to avoid materials inside the FCal which might degrade with time due to radiation damage, these functions were removed to a region of the cryostat where the radiation field is much less. These functions are therefore fulfilled by discrete components.

4.3 The FCal modules

Each of the two Forward Calorimeters at each end of the ATLAS detector (named FCalA and FCalC) consists of three modules, one behind the other. Each module is of similar but not identical construction. The module closest to the Interaction Point (FCal1) is made of copper. The FCal1 module is thought of as an electromagnetic calorimeter. The FCal2 and FCal3 modules are made mostly of tungsten in order to limit the longitudinal and transverse spreading of hadronic showers, providing superior containment but also limiting transverse leakage into cells at lower pseudorapidity where particle energies are typically lower and could be overwhelmed.

The FCal modules are cylindrical in shape with a coaxial hole through which the LHC beams pass. When cold, each module is about 444 mm in depth with an outer radius of about 449 mm. The inner, cylindrical beam-holes increase in radius from one module to the next in proportion to the distance from the IP so they cleanly collimate the spray of min-bias particle debris further downstream, thereby minimizing the radiation backgrounds in the muon chambers. The front face of FCal1 is about 4.7 m from the IP. The FCal1 modules are 28 X0 deep or 2.7 λ. The FCal2 and FCal3 modules are 3.7 λ and 3.6 λ deep respectively for a total active depth of 10 λ. Behind the FCal3 module at each end is a 'plug' of passive brass (Plug3) to help shield the muon system. The three modules and plug at one end of ATLAS are shown in their support tube in figure 7 and the dimensions are summarized in tables 3 and 4. The cavity inside the support tube containing the modules and plug is bounded at the upstream end by the flange on the forward cone (called the "cone end") and at the downstream end by the rear cold bulkhead. Both can be seen in figure 7. From the cryostat drawings [20] we find that the distance from the cryostat outer warm front face to the cone end at room temperature is 1137.5 mm. The present plan is to position the endcap cryostats so that the outer warm front face is at 3540 mm from the IP. If, during cool-down, the rear of the cryostat is constrained, then at liquid argon temperatures the cone end will be 4683.5 mm from the IP.

At the outer periphery of each module are "cable troughs". These are cutouts into which the readout cables are routed from the electrodes to the signal summing boards located at the back of the cryostat volume. The FCal1 electrodes are read out from the side facing the IP while

2008 JINST 3 P02010

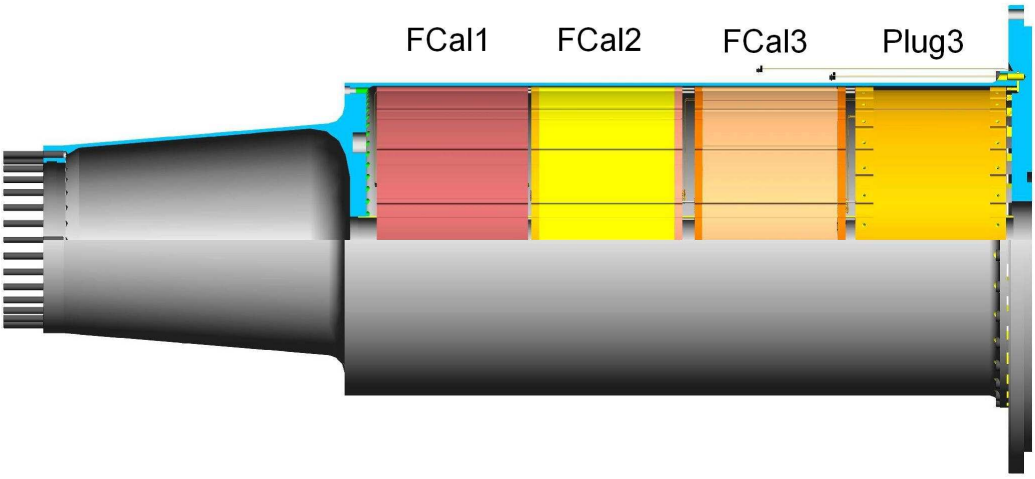

Figure 7. Cut-away side-view of the FCal assembly in the cryostat support tube. The IP is off to the left. From left to right are FCal1, FCal2, FCal3, and Plug3.

the FCal2 and FCal3 modules are read out from the downstream ends. This arrangement is to minimize the radiation exposure to the readout cables, in particular avoiding the region near hadronic shower max between FCal1 and FCal2. There are 16 such troughs on FCal1 and FCal2 to contain the FCal1 readout cables. FCal3 has an additional 8 troughs for the FCal2 readout cables and Plug3 has an additional 4 (for a total of 28) for the FCal3 readout cables. Each trough holds four cable harnesses, each harness containing up to 64 miniature coaxial readout cables. These cables are held in place by copper "trough covers".

In the ATLAS cavern the nominal beam line (lying in the plane of the LHC ring) slopes downward at an angle of about 0.704 degrees to the horizontal when moving around the LHC ring in the counter-clockwise direction as viewed from above. In the ATLAS physics coordinate system the origin is at the IP and the z-axis is along this nominal beam line and points counter-clockwise as viewed from above, i.e. towards downtown Geneva. The x-axis is normal to the nominal beam, lies in the horizontal plane, and points roughly towards the center of the LHC ring. The y-axis is normal to the nominal beam and to the x-axis and therefore points at angle 0.704 degrees from the vertical [21]. At design luminosity the proton bunches in the ATLAS cavern follow a path lying in the y-z plane with angle to the nominal beam of about 150 μradians in the upwards direction, crossing the nominal beam line at the IP ([2], page 257). Therefore each proton has a y-component of momentum of about +1 GeV/c so that the center-of-mass of the incident proton-proton system has a y-component of momentum of about +2 GeV/c.

Each module, with its various groupings of electrodes, has several symmetries about the nominal beam line and the IP. The FCalA and FCalC modules have a parity symmetry about the IP. That is, at position x, y, z on the FCalA one will find an exact upside down mirror image of the feature at -x, -y, -z on the FCalC. Further each module is symmetric under 180 degree rotation about the z-axis. Or, stated another way, each module possesses a parity symmetry in the x-y plane, i.e. at position x, y, z one will find an upside down version of the feature found at -x, -y, z on the same module. And each module on the C-end is mirror symmetric to its corresponding module on the A-end, that is, a feature at x, y, z on a module at the A-end is a mirror image of the feature at x, y, -z on the corresponding module on the C-end. These symmetries apply not only to the electrode locations but also to the tube-group patterns, the readout tile shapes, and the trigger proto-towers. A relatively simple transformation takes the

2008 JINST 3 P02010

FCal Module Parameter	FCal1	FCal2	FCal3	Plug3
Module inner radius (mm)	72.3	78.8	85.7	94.7
Module outer radius (mm)	449.4	449.4	449.4	448.7
Module depth (mm)	444.1	444.1	444.1	442.4
z of front face relative to cone end (mm)	26.4	483.6	965.7	1441.3
$\|\eta\|$ in module x-y mid-plane				
at inner edge	4.92	4.92	4.92	4.90
at outer edge	3.09	3.18	3.26	3.34
Module Mass (kg)	2130	3830	3700	2261

Table 3. Summary of FCal module parameters. Dimensions are at liquid argon temperatures. The plan is to position the End Cap cryostats so that the cone end is 4683.5 mm from the IP. Module masses are measured values averaged over the A and C ends.

Front End Board channel number for a readout tile located at x, y, z on the A-end to the Front End Board channel number for the mirror image readout tile located at x, y, -z on the C-end.

The electrode hole pattern is offset so that, if continued down to the origin in the x-y plane, the origin would fall on the midpoint between two neighbor electrodes, one in the row just below the midplane and the other in the adjacent row just above the midplane. This means that no hole centers fall on the boundaries between quadrants, they all clearly fall into a quadrant.

During ATLAS operations the cryostat temperature is maintained a bit below 90 K by cooling loops located just inside the outer periphery of the cold vessel. These cooling loops are far from the FCal which must be cooled by heat transfer through the surrounding detectors, cryostat structures, and liquid argon. In the vicinity of the FCal the pressure of the liquid argon is about 1.8 bar resulting in a boiling point of about 92.7K. Heat sources and heat flow in the region of the FCal have been studied to determine the maximum temperature rise to ensure we do not have boiling within the FCal. The FCal sits inside the HEC and the HEC modules are constructed with copper plates which are continuous in radius. This results in very efficient heat transfer which produces a temperature drop of less than 0.1K across the HEC for the heat load associated with full LHC luminosity. For this reason we assume, as a boundary condition for our heat studies, that the inner radius of the HEC is at the same constant temperature maintained by the cooling loops.

Monte Carlo simulations have indicated that at the LHC design luminosity the heat load due to energy loss by particles from min-bias events on each set of FCal modules could be as high as 45 Watts. This is a conservative estimate and has been used to estimate the maximum temperature rise in the FCal system. Over two thirds of the energy from min-bias events is deposited in the FCal1. When the HV is turned on, another 9 Watts is deposited in the liquid argon in the FCal1 due to the drifting electrons and positive charges. In addition to the beam related heating, the FCal is affected by a heat leak through the cryostat wall at its inner radius. The gap between the cryostat warm and cold walls is smaller (16.5 mm) in this region than in other parts of the cryostat. In initial tests of the cryostat, the heat leak through this region caused condensation on the outside warm wall of the cryostat in the region of the FCal. To prevent this, heaters were attached to the warm wall. This arrangement was tested with the cryostat cold by monitoring the temperature of the cold and warm walls with a set of twenty-four temperature sensors. Analysis of these data led to the conclusion that the heat leak was less than 10 W/m^2 for a total heat leak of approximately 5 Watts.

2008 JINST 3 P02010

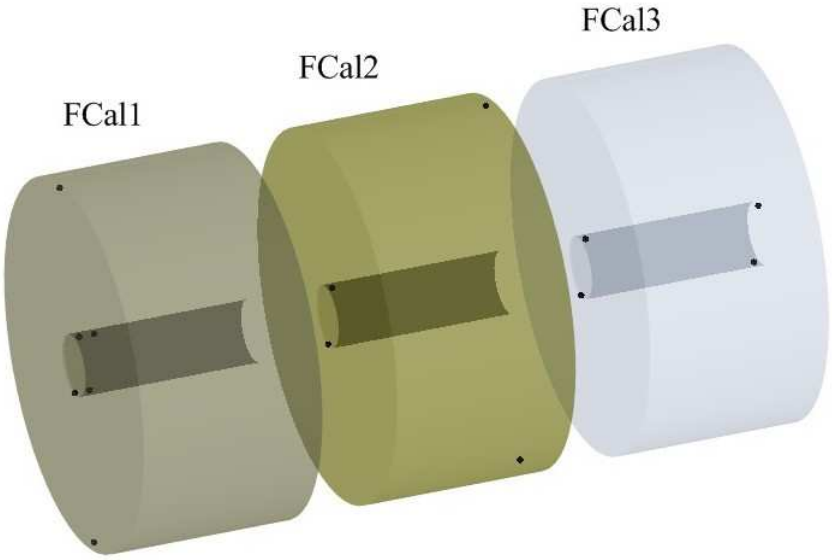

Figure 8. Diagram of location of temperature monitoring points, indicated by black dots. All sensors are in the end plates of the modules except for two sensors at the inner radius of FCal 1 which are located at a depth of 10 cm (in z) into the modules.

With the knowledge of the heat inputs it was possible to model the heat flow in the FCal and estimate the maximum temperature rise. To make the analysis more tractable, the problem was broken into steps. The FCal modules are composite objects, so effective thermal conductivities were calculated for each of the three FCal modules using a Finite Element Analysis (FEA) of the detailed structure of the modules. It was assumed that conductivity was the dominant form of heat transfer except in the large liquid argon filled gaps between the FCal support tube and the HEC and also between the inner radii of the FCal modules and the cold wall of the cryostat. In these regions convection and conduction were modeled using an FEA. This was then used to calculate an effective conductivity for these regions of liquid argon. All this information was then used in a three dimensional FEA of the FCal region to calculate the maximum temperature rise which occurs near the inner radius of FCal1. At full LHC luminosity this was estimated to be less than 1.5 K which indicates that boiling will not be a problem. It should be noted that the temperature drop from the hottest FCal1 electrode rod to its corresponding tube, assuming only conductive heat flow across the liquid argon gap, is about 11 mK. So this kind of localized heating above the maximum calculated by the FEA can be neglected.

The temperature of the FCal modules during the ATLAS operational phase will be monitored by a set of 14 temperature sensors in each set of FCal modules [22] as shown in figure 8. The output of these at different LHC operating conditions can be compared with the temperature rise predicted by the FEA calculation. This will allow fine tuning of the FEA study to make better predictions for future operating conditions such as those that will be encountered with higher luminosities anticipated with the LHC upgrades.

4.4 The unit cell

We can think of each FCal module as made up of identical unit cells. Each unit cell is parallel to the beam (z) axis, extends the full length of the module, and contains within it one liquid argon electrode. It also contains the absorber material associated with that cell. To first approximation, each cell is uniform in depth but has structure in the x- and y-directions. It is convenient to think

2008 JINST 3 P02010

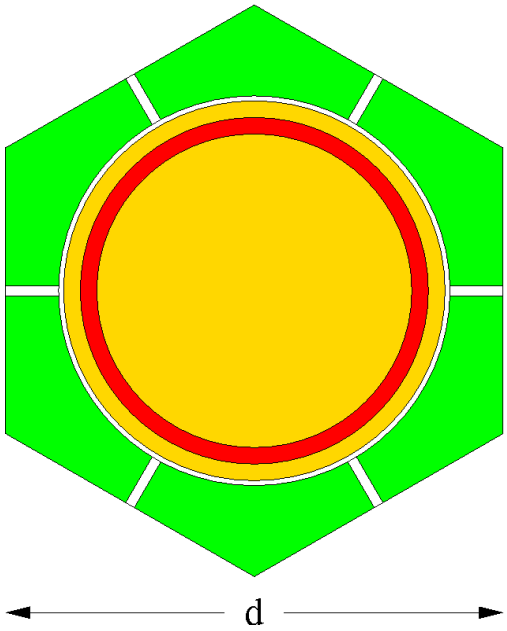

Figure 9. FCal Module Unit Cell. This cross section shows, from the center outwards, the electrode rod (yellow), the liquid argon gap (red), the electrode tube (yellow), the tolerance gap (white) between the OD of the tube and the absorber matrix, and the absorber matrix (green). In the case of FCal2 and 3 there are also tolerance gaps between the tungsten alloy matrix slugs as shown here.

of each module as built up with a repeating pattern of such cells. This simple description breaks down at the inner and outer radii of the modules. There is additional material between the boundary of the region covered by unit cells and the inner and outer cylindrical surfaces of each module; for FCal2 and FCal3, those unit cells on the boundary have some fraction of the tungsten alloy slugs replaced by copper.

The major features of the unit cell are shown in figure 9. Of the several shapes allowed for the unit cell, the hexagon has the most symmetry. The axis of the electrode rod is coaxial with the center line of the cell. The liquid argon gap (shown in red) lies between the rod and the electrode tube. Extending to the cell boundary is the matrix (shown in green) which is copper for FCal1 and tungsten alloy for FCal2 and FCal3. Between the tube and the matrix is a tolerance gap which fills with liquid argon. Here the gap is shown as a ring but in reality the tube and matrix typically touch somewhere around that gap leaving a larger gap on the far side. For FCal2 and FCal3 there are also tolerance gaps between the tungsten alloy slugs, shown in the figure as uniformly distributed. Again the tolerance gaps are usually close at some boundaries leaving larger gaps at other boundaries. Because the tolerance gaps are small, the non-uniformities due to their uneven distribution are also small.

The unit cell is not perfectly uniform along its length. For all the modules, the signal end plate has a smaller tolerance gap between tube and matrix. And part way through the end plate the tube is swaged into a feature machined in the electrode hole to make a robust ground contact (figure 6). For each of the two FCal2 and FCal3 modules the two copper endplates displace the tungsten alloy matrix with copper and some electrode tubes are swaged at both ends. And because the tungsten alloy slugs are between 6 and 10 mm long, the longitudinal gaps between slugs add to the tolerance gaps which fill with liquid argon.

Summary parameters for the unit cells in the three modules can be found in table 4.

2008 JINST 3 P02010

FCal Unit Cell Parameter	FCal1	FCal2	FCal3
Electrode spacing (mm)	7.50	8.18	9.00
Material			
Rod	Cu	W	W
Tube	Cu	Cu	Cu
Matrix between End Plates	Cu	HM	HM
EndPlate	Cu	Cu	Cu
Unit Cell volume ratios (%)			
Rod	35.80	32.95	33.81
LAr Gap	8.54	10.67	13.40
PEEK Fiber	0.10	0.17	0.24
Tube	8.94	7.91	7.57
Matrix between End Plates	38.07	37.54	35.28
End Plates	4.99	4.90	4.56
Interstitial spaces	3.56	5.87	5.14
Unit Cell Density (g/cc)	7.87	14.28	13.97
dE/dx Sampling fraction (%)	1.61	1.33	1.70
Sampling frequency (cm^{-1})	3.2	2.8	2.6
Depth (X0)	27.6	89.7	88.0
Depth (λ)	2.65	3.62	3.55
Moliere radius (mm)	17.1	11.9	12.1

Table 4. FCal unit cell parameters, warm values. HM is an alloy of 97% W by weight.

4.5 The FCal1 module

The backgrounds from min-bias events in the FCal1 module are particularly large. Neutral pions in these min-bias events decay to photons which create EM showers in the FCal1 module. The highest ionization rate per unit volume is near EM shower max at the highest value of $|\eta|$ before transverse shower leakage down the beam hole becomes significant. At the nominal LHC luminosity at $|\eta| = 4.67$ (about 19 mm from the inner edge of FCal1) at a depth near EM shower max the deposited power density in the calorimeter averaged over bunch crossings is about 15 TeV/mm^3/s corresponding to about 3.0 MGy/LHC yr. The deposited power density in the liquid argon at this same position is about 2.6 TeV/mm^3/s, giving an ionization rate of 18 nC/mm^3/s of each charge sign. At $|\eta| = 3.3$ the ionization rate falls to about 0.3 nC/mm^3/s. For reference, the critical ionization rate is D_c = 96 nC/mm^3/s [15]. Hadronic showers from min-bias events are spread out in depth so the ionization density is lower.

At a distance from the IP corresponding to EM shower max in FCal1, the radius of a QCD jet cone of R = 0.4 is about 36 mm at $|\eta| = 4.67$ while at $|\eta| = 3.3$ it is about 143 mm, a factor 4 larger. The jet energy is deposited over a larger radius due to shower spreading.

From the above we see that external conditions change rapidly across the face of the FCal. Yet it is imperative that the module be uniform in all respects so that energy calibration can be accurately determined and maintained. Thus the properties of the unit cell, containing one electrode, are kept consistent throughout the calorimeter by tight production tolerances.

The material of FCal1 is nearly all copper. Copper was chosen for two principal reasons. 1) The Molière radius (17 mm) is large enough to ensure that the response across the front face of the module is reasonably uniform. That is, the size of an EM shower is comfortably larger than

2008 JINST 3 P02010

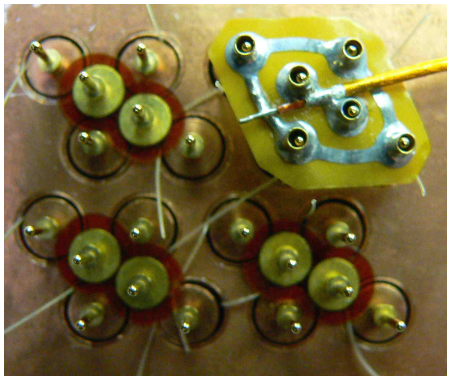

Figure 10. FCal1 interconnect with sockets which mate with the signal and ground pins from the liquid argon electrodes. Also shown is the Axon miniature coaxial cable which takes the signal from the module to the summing board.

the transverse feature size of a unit cell (table 4). 2) Copper allows the heat deposited in the FCal1 modules, primarily from min-bias particle showers, to be removed efficiently to avoid large temperature differentials which could cause the liquid argon to boil in the gaps. In particular, the matrix plates are C11000 pure copper. The electrode tubes are UNS alloy C12200. The electrode rods are C11000 copper H80 (hard drawn). The PEEK monofilament insulating fiber is the only other material within the module near EM shower max [23].

The FCal1C (FCal1A) matrix is composed of 18 (19) copper plates with identical hole patterns. The 12,260 holes for the electrodes in each plate were required to line up with good precision so that the clearance was minimized. This was to minimize the volume of argon between the outer diameter (OD) of the electrode tube and the inner diameter (ID) of the hole in the matrix. The holes in all but the readout plate had a clearance of about 0.1 mm. The holes in the readout plate were slightly smaller, and therefore the fit to the electrode tube tighter, so that the swage for the ground connection would be robust.

Each matrix plate was aligned with its neighbor by one short, stainless steel dowel pin, 20 mm long and 5 mm in diameter, and one short, stainless steel, rolled spring pin, 20 mm long and 6.5 mm in diameter before compression, both located near the outer periphery on opposite sides of the module.

The matrix plates are held together by four stainless steel 5 mm diameter “tie rods” at the outer periphery of the module. The hex head of each rod is recessed in the readout matrix plate. A spring washer was inserted on the shank at the head to maintain stress in the shank. The far, threaded end was screwed into a HeliCoil [24] fixture embedded in the far end plate. Tests of the HeliCoil in copper plate showed that it would not pull out of the plate with 40 kN of force. The tie rods were screwed in with a torque of 10 Nm and then the head was backed off to relieve the torsional stress in the shank. By calculation, each tie rod was left with an axial stress of 1000 N at liquid argon temperatures. The frictional shear force between plates is sufficient to maintain the structural integrity of the module when supported only by the two end plates. The 12,260 electrode tubes provide additional resistance to shear.

The electrode signal and ground pins are gold-plated yellow brass [25]. Details of the features on the pin can be seen in the drawing of figure 3. The shank of the pin which fits inside the hole has barbs to hold it in place and to make a firm electrical connection. A signal pin was press-fit into a hole in one end of each electrode rod. Two ground pins were press-fit into similar holes in the matrix end plate for each of four electrodes as seen in figure 5 and figure 10.

2008 JINST 3 P02010

The ground pins also hold the polyimide washers which prevent the electrode rods from working out of their tubes. The polyimide washers were backed by smaller brass washers to provide added strength. Ground pins were also mounted in the far matrix end plate solely to hold the electrode rods in place with identical washers to the signal end. The shaft on the pin designed to fit into the interconnect socket was cut off the ground pin at the far end.

The FCal1 interconnect boards (figure 10) are made of thin, flexible polyimide sheet with glueless copper traces. Four signal sockets and two ground sockets [26] are soldered to each board and mate to the pattern of pins on the four electrodes and two ground pins in the matrix.

On delivery, the copper matrix plates were visually inspected, weighed, and the electrode holes were subjected to a go/no-go gauge to check that the diameter tolerance was met. Samples of the copper tubes and rods were measured via a production procedure and all measurements recorded for the metrology mentioned in an earlier section. Signal pin holes were drilled in the ends of the rods. The ends of the rods and tubes were de-burred. Then the tubes and rods were soaked for several days in acetone. The matrix plates were sprayed with a high-pressure solution of LPS in water to degrease the surfaces, the electrode holes, and the ground pin holes. The tubes, rods, and plates were then subjected to a warm ultrasonic bath of LPS solution, rinsed in de-ionized water, cleaned in an ultrasonic bath of Citrinox to remove oxides, rinsed in de-ionized water again, then dipped in two successively purer ethanol rinses, and then blow-dried with nitrogen gas. While the matrix plates were in the ultrasonic LPS and Citrinox solutions the ground pin holes were swabbed with microbrushes. Just before the ethanol rinses the matrix plates were briefly dipped in LPS again. The tubes and rods were stored in double-wrapped plastic bags purged with Nitrogen gas while awaiting insertion into the matrix.

The matrix plates were stacked on edge on a cradle which was equipped with two “feet” for each plate. These feet were screw-adjustable to hold the plate in alignment with the adjacent plates. When each plate was in alignment with the previously stacked plates, clamps pulled it flush as the dowel pin and spring pin engaged. After all plates were stacked the four tie-rods were inserted with their spring washers and tightened as described earlier. Next the tubes were inserted and swaged at the signal end. Finally the rods were inserted in a screw fashion as the PEEK fiber was wrapped around. The PEEK fiber was cleaned with ethanol as it was unwound from the spool. After every two rows of rods were inserted, each electrode was HV tested to insure that there was no current draw. For those few rods with excessive current draw, the rod was pulled, cleaned with alcohol, the tube was swabbed with alcohol, and the rod re-inserted and tested again.

4.6 The FCal2 and FCal3 modules

The ATLAS Forward Calorimeter was required to have dense hadronic modules as described earlier. These requirements were met by using tungsten as the absorber material. Tungsten is a refractory material and is difficult to machine. Industrial methods exist to make small parts with complex shapes out of tungsten and also to make much larger tungsten rods. These constraints drove the design of the absorber matrix for FCal2 and FCal3 which is shown schematically in figure 11. This figure shows the electrode structure consisting of a copper tube that contains a tungsten rod with an anode pin fitted into the end. The electrodes are surrounded by a large number of tungsten slugs that fill the space between the tubes in a hexagonal pattern. The slugs, which are 1cm long, are shown in detail in the photograph of a mockup in figure 12.

2008 JINST 3 P02010

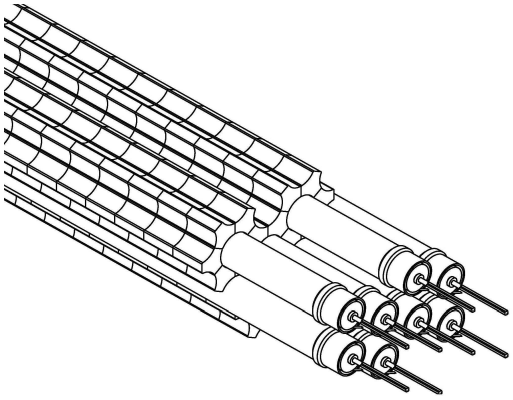

Figure 11. Schematic drawing of FCal hadronic calorimeter showing slugs, tubes, rods, and anode pins.

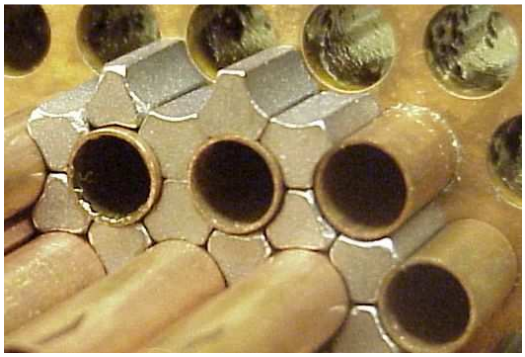

Figure 12. Photograph showing a mockup of the arrangement of tungsten slugs around the copper electrode tubes.

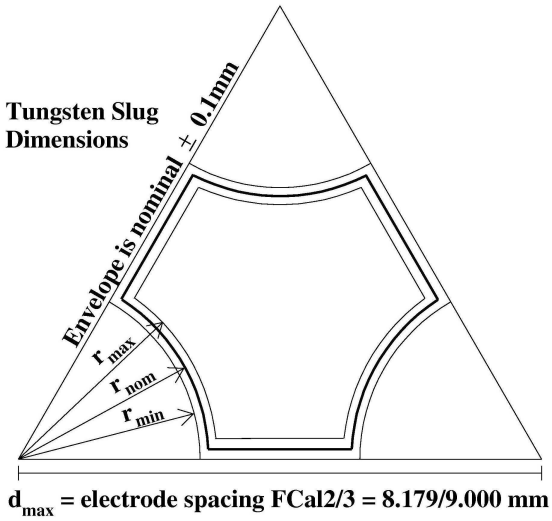

Figure 13. Diagram of slug dimensions showing tolerance bands. The bounding triangle has sides of length d_{max} and the slug must be outside the arc of radius r_{min} from each triangle apex.

All tungsten parts are produced by sintering powdered tungsten with or without additional powdered binder materials. Rods were produced of pure tungsten as additional post sintering steps that are used to compress and form the rod at high temperature produce a high density rigid structure without the need for binder materials. Once formed in this way the rods are machined using centerless grinding to produce a precision rod of the required diameter and surface finish. The density of the rods used in the FCal detectors was 19.2 g/cm^3. The FCal tungsten alloy slugs were made by compressing a mixture of 97% tungsten powder with 2% nickel and 1% iron by weight as binder materials in a mold to produce "greenform" parts. At this stage the parts also contained an organic binder which burned off when the parts were fired in a high temperature oven. The temperature was high enough to melt the iron and nickel, binding the tungsten powder and resulted in a shrinkage of approximately 20%. The density of the final slugs was 18.3 g/cm^3. The critical part in the commercial slug manufacture was the control of tolerances. Figure 13 shows a drawing of the slug cross section. The nominal slug size is shown by the darker line. The tolerance lines are also shown at ± 0.1 mm at 90° to the surface. Initial shipments of FCal3 slugs were oversized (average triangle size of 9.01 mm). It

2008 JINST 3 P02010

	FCal2	FCal3
d_max	8.18	9.00
r_min	3.09	3.50

Table 5. Specifications for slug dimensions in mm.

was decided that these slugs, representing 32% of the total, could be accepted, provided that the remainder of the slugs were made slightly undersize. The two samples were mixed uniformly. For FCal2 and FCal3, problems with quality control with the initial shipments lead to a vendor change partway through the production. The slugs for FCal2 from the two companies had a 5% difference in average mass per unit length. Because this change occurred during stacking, the first module (FCal2C) uses dominantly slugs from the initial vendor while the FCal2A module was stacked mainly with slugs from the second vender plus those remaining from the first. This accounts for most of the difference in the masses of the two modules (table 6).

The mechanical structure of the hadronic FCal modules consists of 23.5 mm thick copper endplates separated by copper cladding plates at the inner and outer radii, sometimes called inner and outer absorbers. The endplates have 10200 (8224) through holes in FCal2 (FCal3) for the electrodes. In both FCal2 and FCal3 the signals from the electrodes are read out by connections at the signal endplate which is the one furthest from the IP. The electrodes consist of a tungsten rod and a copper tube, separated by a PEEK fibre wound round the rod. All the copper tubes are swaged into shaped grooves in the signal endplates to form a good electrical contact, whilst the tubes at the inner and outer radii (in total 41 rows) are swaged at both ends to provide structural rigidity. The overall final structural integrity of the modules is formed by the endplates, the double swaged tubes and the inner and outer cladding plates. The spaces between the tubes are filled with tungsten slugs that are dimensioned to give a non-interference fit. The tungsten rods are much more rigid than the copper tubes and when installed with the close fitting PEEK fibers add strength to the modules.

The modules were constructed on an assembly stand (figure 14) that allowed rotation and height adjustment. The first step in the module assembly process was to mount the one piece inner cladding and copper endplates on the assembly stand (figure 14) and install six spacer bars between the endplates at large radius. The inner cladding and the spacers were used to fix the endplate separation and hence the overall module dimensions. The absorber matrix was then installed radially outward from the center, a layer of slugs followed by a layer of tubes in a phi sector (figure 14), followed by a rotation to the next sector. Each FCal2 (FCal3) module contained approximately 800k (640k) slugs which were laid into a line using a custom rotary bowl feeder. The line of slugs was then fed into place between two copper tubes within the module using a shaped tube. Each row of slugs was completed using a slug selected from a manufactured set of short slugs to provide a gap of 1-2 mm to allow for differential expansion along the row. (The copper structure contracts more than the row of tungsten slugs during cooling to liquid argon temperatures.)

The mechanical structure of the modules was completed with the addition of 12 outer cladding plates which have cutouts on the outer radius for cable troughs, as can be seen in figure 15. There are 16 cable troughs in the FCal2 modules and 24 in the FCal3 modules. Both the inner and outer cladding plates have crenellated interior surfaces to mate smoothly with the tube and slug pattern of the absorber matrix. The crenellated surface of the inner absorber can be seen in the upper left of figure 14.

2008 JINST 3 P02010

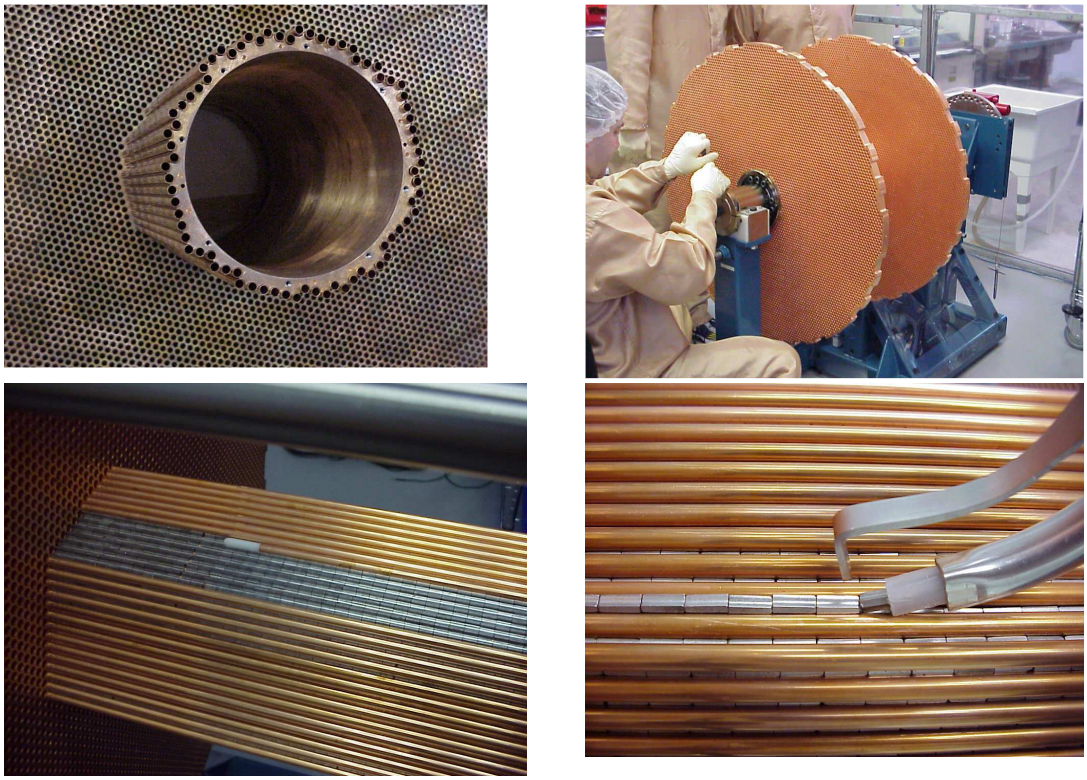

Figure 14. Construction of hadronic FCal modules. Top-left: Inner cladding with one layer of tubes and one end plate. Top-right: Endplates mounted and aligned on the module assembly tooling. Bottom left: matrix stacking – insertion of tube over row of slugs. Bottom right: laying a row of slugs using the slug feeding tooling.

Electrical connection to the tungsten rod is made using gold plated brass pins [27] that were press-fit into a hole drilled in the centre of the tungsten rod. PEEK fibres were wrapped around each rod with 8 ± 1 turns (see figure 16) and then the PEEK was thermoformed by heating to 170 C for 8 minutes. The rods, complete with wound fibers, were then inserted into the tubes. In some cases the tolerance build-up of tube, rod and fiber resulted in a tight fit. In these cases a different rod was tried or the rod was wound with a slightly undersized fiber and reinserted. Ground connections are normally made with 4 (8) MillMax pins [28] per tube group for FCal2 (FCal3) which were inserted with a press-fit into holes in the endplates. These ground pins hold small PEEK retention washers in place against the endplates using smaller split washers that snap over barbs on the pins. The retention washers constrain the rods and prevent the PEEK fiber from unwinding. At the non-readout end, retention pins [29], identical to the ground pins except without the shaft which mates to a socket, hold identical retention washers. The pins and washers can be seen in figure 17 and figure 18.

Thin polyimide printed circuit "interconnect" boards are used to gang anodes together into tube groups of 6 (9) tubes for FCal2 (FCal3) as can be seen in figure 18. Each board has a miniature coax cable attached that is used to read the signals out and provide high voltage. The connections to the signal pins and ground pins are made via an array of sockets [30] mounted on each interconnect board. Most of the face of each module is tiled with a standard shape board, while irregular boards with a number of different shapes are used at the inner and outer edges of the modules. The interconnect boards were installed on the modules after the tube capacitance measurements were completed. The capacitance of each tube group was measured after the boards were installed.

2008 JINST 3 P02010

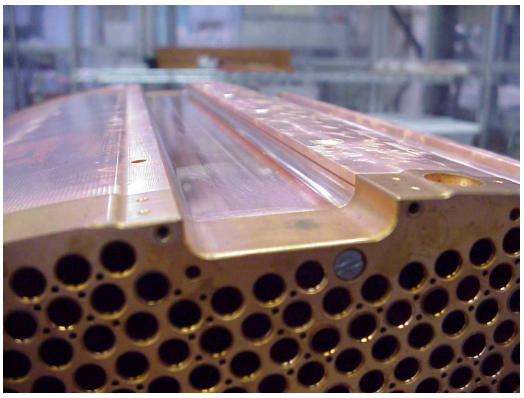

Figure 15. Photo showing endplate and outer cladding plate with cut out for cable trough.

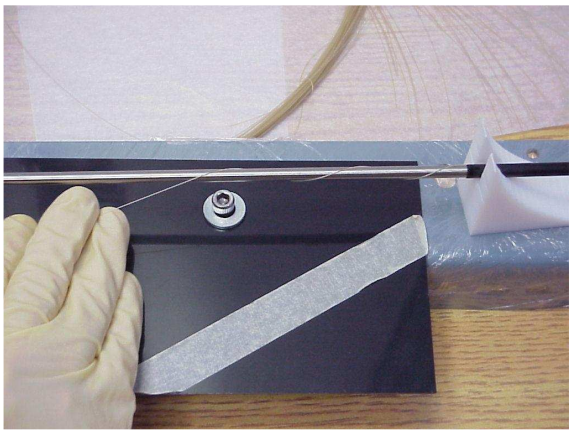

Figure 16. Winding of PEEK fiber on tungsten rod prior to thermo-forming.

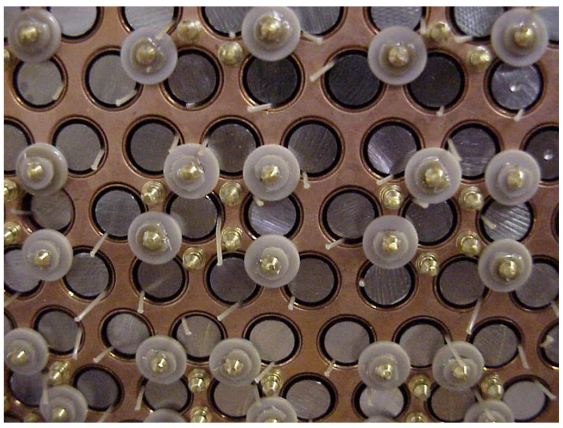

Figure 17. Photo at the non-readout end of FCal3 showing ground pins with retaining washers.

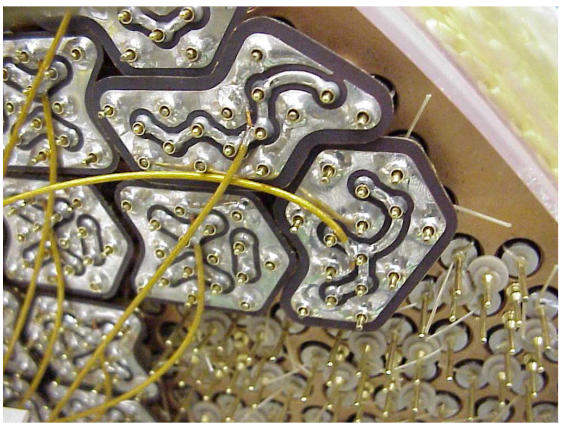

Figure 18. Photo showing both regular and irregular interconnect boards mounted on signal and ground pins of FCal3.

Quality control checks were made on all components for the module including mass, and dimensions. All components were cleaned in an ultrasonic bath following a defined multi step cleaning process. This was done to minimize the amount of metal particulate on the components as this was found, from our prototyping experience, to be a major cause of electrode failure due to electrical breakdowns. Particular attention was paid to the preparation of both the copper tubes and the endplates. It was necessary both to remove burrs from the ends of the tubes and ensure that the inner surface of every tube was free of metal particulate. The holes in the endplates had to be treated with similar care. After the insertion of the tungsten rods into the tubes a series of tests at up to the nominal operating voltage were made to ensure no electrical short was present. Electrode shorts were corrected up to the point of final assembly of the FCal modules.

Dimensions of the modules are provided in table 3 and table 4. The masses of the components used in the FCal2 and FCal3 modules are provided in table 6.

The ATLAS Monte Carlo simulation requires as input the materials and densities of all the components of the detectors. The materials of the FCal2 and FCal3 unit cells were modeled as three regions, the tungsten rods, the active liquid argon gap and the absorber matrix which is everything not in the first two categories. The mass fractions of the materials in the absorber matrix are derived from the numbers in table 6 and are shown in table 7. The materials include

2008 JINST 3 P02010

	FCal2A	FCal2C	FCal3A	FCal3C
Endplate 1	59	59	58	55
Endplate 2	59	59	57	55
Inner Cladding	11	11	18	18
Outer Cladding	71	71	92	92
Tubes	185	200	179	179
Slugs	1737	1801	1624	1626
Rods	1656	1662	1664	1664
Other parts	8	8	8	8
Total	3786	3871	3700	3697

Table 6. Mass of components used in FCal2 and FCal3 in kg.

	FCal2	FCal3
Copper	0.15	0.15
Tungsten alloy	0.84	0.84
Liquid Argon	0.01	0.01
Absorber density	14.37	14.45

Table 7. Mass fractions and densities (in g/cm^3) of the absorber matrix, derived from construction information, averaged over ends, and input into the Monte Carlo.

the copper tubes, the tungsten alloy slugs, and the liquid argon filling the tolerance gaps. The matrix density is for unit cells which are not at the inner or outer boundaries. For these boundary unit cells some of the tungsten slugs are replaced with the copper of the cladding, giving a smaller density. The densities are calculated using the numbers in table 3, table 4 and table 6.

5. The electrical signal

In each electrode, the tube is held at ground and the rod at a positive high voltage such that the electric field in the gap is approximately 1.0 kV/mm, the nominal field for most liquid argon sampling calorimeters. The shower particles ionize the liquid argon and the resulting electrons drift to the rod creating a current pulse. The transverse size of each electrode is small compared to the transverse size of an electromagnetic or hadronic shower. Therefore at any depth along the electrode the ionization across the gap is nearly uniform. This produces a current pulse which is nearly triangular in time with a sharp rise (less than approximately 1 ns) followed by a linear drop back to zero in the time it takes for the last electrons to drift across the gap (~ 61 ns in FCal1) [17].

The FCal electrodes act like short (1.8 ns) transmission lines, open at one end and connected to a readout coaxial cable at the other. Because the characteristic impedance of the electrodes, ganged together in parallel at the interconnect, is so low, it is not possible to match them to the readout coax. Hence the triangle current pulse reflects back and forth many times on the electrodes, diminishing in amplitude with each reflection as part of the pulse is transmitted to the cable [31]. It is a reasonable approximation to treat the tube group as a discrete capacitance (C_D ~ 1.5 nF) discharging into the coaxial cable characteristic impedance Z with

2008 JINST 3 P02010

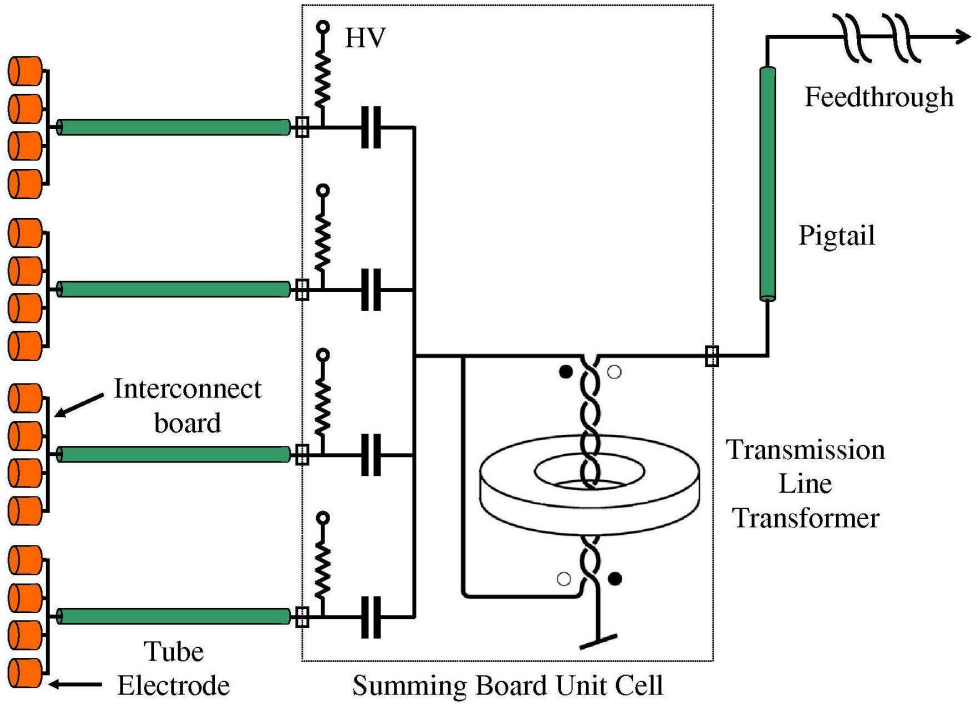

Figure 19. The FCal electronics chain. Sixteen electrodes are shown as short orange tubes on the left. Equal length coaxial cables take the signals to a "summing board" where protection resistors introduce HV to the electrodes and blocking capacitors isolate the HV from the remainder of the circuit. The twisted pair transmission line in the transformer is wrapped around the ferrite core 8 times (wrapping not shown).

characteristic time $\tau = ZC_D$. A low characteristic impedance leads to a shorter pulse with a larger pulse peak relative to the electronics noise. The lowest practical choice was $Z = 25\ \Omega$ giving $\tau \sim 38$ ns. The current pulse on the readout cable is approximated by the convolution of the triangle pulse with a decaying exponential.

The connection of the electrodes to the readout coaxial cable at the interconnect is highly uniform. The swage of the electrode tubes into the copper endplate to make a positive electrical connection and the ground pins located very near to the tube group ensure a low inductance ground connection. In a given module all of the readout coaxial cables are the same length.

The readout cable carries the current pulse to a "summing board" (figure 19). These boards are mounted behind the Hadronic EndCap (HEC) Calorimeter (figure 20) where radiation levels are much lower than in the region of the FCal. The summing board performs two functions: 1) HV distribution and 2) signal summing.

HV is applied to each tube group down the coaxial readout cable. That is, the readout cable serves two functions; carrying the signal away from the module and supplying HV to the electrodes. Each of the four tube groups shown in figure 19 is fed from a different HV supply. In case of a HV failure only one tube group in a readout tile is affected. The potential is applied through a protection resistor on the summing board which limits the current in case of a spark or short in an electrode. For electrodes at a large radius from the beam centerline we use a 2.0 MΩ resistor while at smaller radii we use a 1.0 MΩ resistor. These resistors [32] are rated at 2.0 kV, and have an almost negligible temperature dependence. Blocking capacitors a.c. couple the signal to the summing circuit. These 12 nF capacitors [33] are rated at 500 V for FCal1 and FCal2 and 1.0 kV for FCal3.

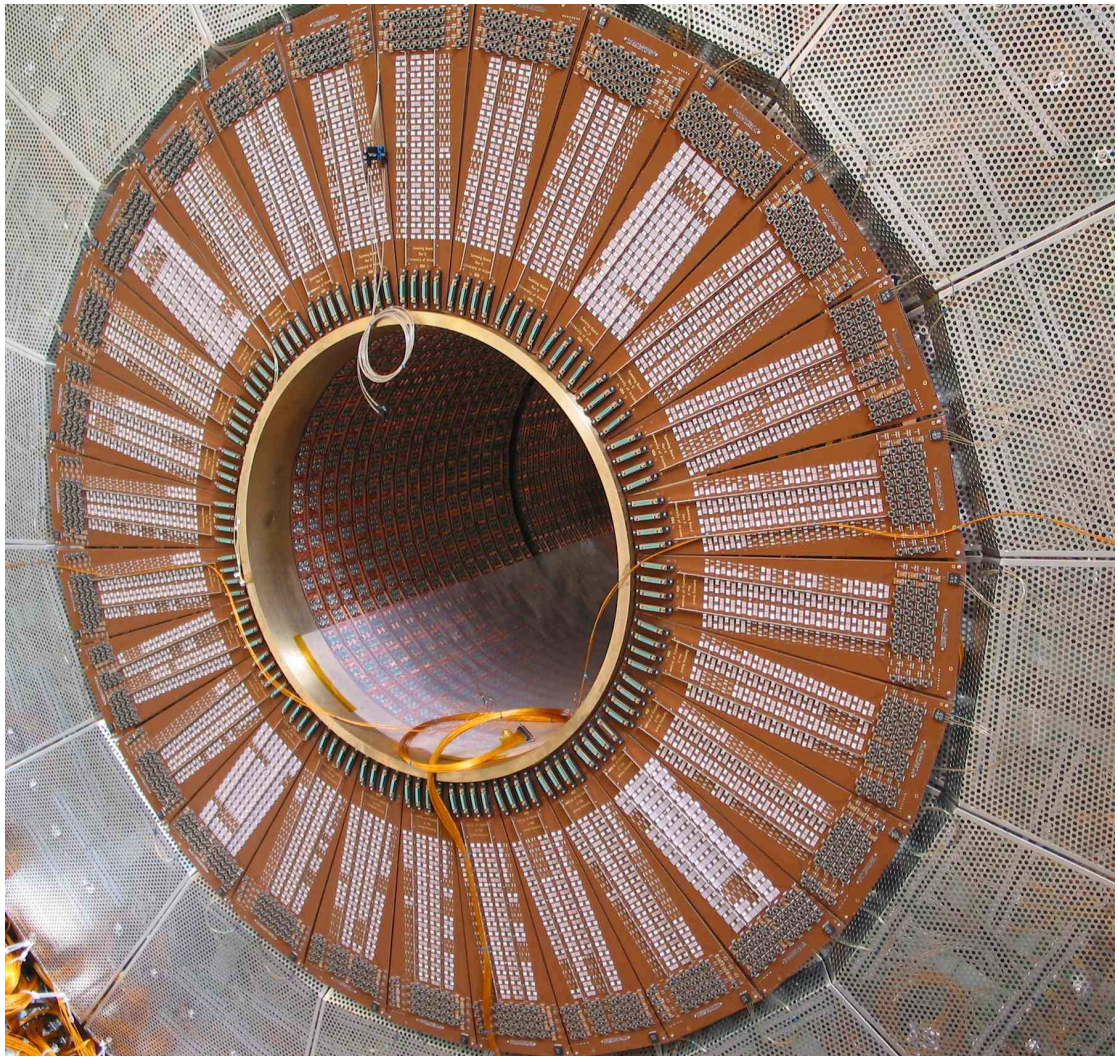

Figure 20. The 28 FCal summing boards are mounted on the rear of the HEC calorimeter before the FCal is inserted into the EndCap cryostat.

Four signals, delivered to the summing board by the readout cables, are summed together via a transmission line transformer [34]. This passive device matches the impedance of the four coaxial cables in parallel (6.25 Ω) to the pigtail coaxial cable (25 Ω) over the frequency range from about 100 kHz to 250 MHz, much wider than the band-pass of the subsequent warm electronics. The current is halved and the voltage doubled in this summing process. Power losses are negligible and the electronics noise current is the same as for a single tube group. The transformer uses a low permeability ferrite core (3D3) so that it can operate in the fringe field of the ATLAS solenoid magnet without degradation due to saturation effects. Wound around the core are eight turns of a 13.7 cm long 50 Ω twisted pair with polyimide insulation [35]. The core is oriented so that its axis is roughly parallel to the fringe field. The connections (but not the windings) are indicated in figure 19.

Most, but not all, tube groups are summed in this way to make a readout tile (sometimes called a readout channel). Tube groups near the inner and outer periphery of each module are not summed because the geometry of the resulting readout tile would be awkward. For those unsummed tube groups which are later mixed in the shaper along with summed tiles to make

2008 JINST 3 P02010

	FCAL1	FCal2	FCal3
Electrode			
Gap g (mm)	0.269	0.376	0.508
The shorter of Tube or Rod length			
Warm L_w (mm)	445.0	443.5	443.4
Cold L_c (mm)	443.7	443.1	443.0
Cold t_T (ns)	1.82	1.82	1.82
Capacitance (pF)			
In air (measured)	236.1	177.2	150.0
Contribution of PEEK fiber	4.7	4.7	5.9
In LAr C_E	354.1	265.2	223.5
Characteristic Impedance in LAr (Ω)	5.22	6.90	8.21
Number of electrodes ganged at interconnect n_g	4	6	9
Ganged capacitance in LAr C_D (pF)	1416	1591	2012
Ganged characteristic impedance in LAr (Ω)	1.31	1.73	2.05
Readout cable (cold cable harness)			
Length (m)	3.10	2.25	2.10
Propagation delay (ns)	20.7	15.0	14.0
Sampling Fraction for Min Ionizing Particles f_S (%)	1.58	1.30	1.65
'e' to 'mip' ratio r(e/mip)	0.90	0.68	0.68
'e' to 'π' ratio r(e/π) at 200 GeV	1.23	1.20	1.20
Voltage across the gap V (volts)	250	375	500
Drift time across the gap t_{dr} (ns) @ actual E-field	61.0	81.7	113.1
Pileup Penalty (%)	19	36	45
Peak of pulse per deposited energy on EM scale			
Initial current on triangle pulse i_0 (μA/GeV)	-1.494	-0.693	-0.636
Current into preamp i_{in} (μA/GeV) [Includes ZC_D integration, loss at blocking capacitor, halving in transformer, and ohmic losses on cable]	-0.277	-0.137	-0.128
ADC output R_S at high gain (ADC counts/GeV)	20.7	9.9	8.8
Electronics noise rms amplitude on high gain N_S (ADC counts)	5.2	5.2	5.2
Max energy in readout cell (TeV)	5.1	10.9	12.6

Table 8. FCal electrical parameters.

trigger sums, we divide the current by a factor two with a "π" resistor network which looks like 25 Ω from either side. (There is an electronics noise penalty for these tube groups.) Each resistor network is mounted on the summing board where a transmission line transformer would normally sit. Many unsummed tube groups are mixed in the trigger branch only with other unsummed tube groups so, in this case, no attenuation is required. For the resulting readout channels the gain is twice that shown in table 8.

From the summing board each tile signal is carried by a 4.3 m, 25 Ω coaxial cable called a "pigtail". This cable is identical to those in the cold cable harnesses. This pigtail brings the signal to the cryostat feedthrough. The feedthrough has a cold connector and a warm connector with a 41 cm, 42 Ω stripline [36] between. Another 28.5 cm, 42 Ω stripline (pedestal cable) [36] takes the signal from the warm connector on the feedthrough to the warm, front-end electronics mounted at the downstream outer periphery of the cryostat. See figure 1.

On each endcap cryostat are mounted 13 Front End Crates (FEC). One such crate at the top of each cryostat houses the front-end electronics for the FCal. The pedestal cable is connected on one side of a baseplane and the Front End Board plugs into the other side.

	FCal1	FCal2	FCal3
For each of the two FCals			
Number of electrodes	12,260	10,200	8,224
Number of interconnects	3,066	1,700	914
Number of cable harnesses	64	32	16
Number of summing boards	16	8	4
Number of pigtails	16	8	4
Number of Front End Boards	8	4	2
Number of Readout Channels	1008	500	254
Number of HV Channels	64	32	16
Number of Layer Sum Boards	16	8	4
Number of trigger proto-towers	64	64	64

Table 9. Multiplicity of various elements of the electrical system for each of the two FCals.

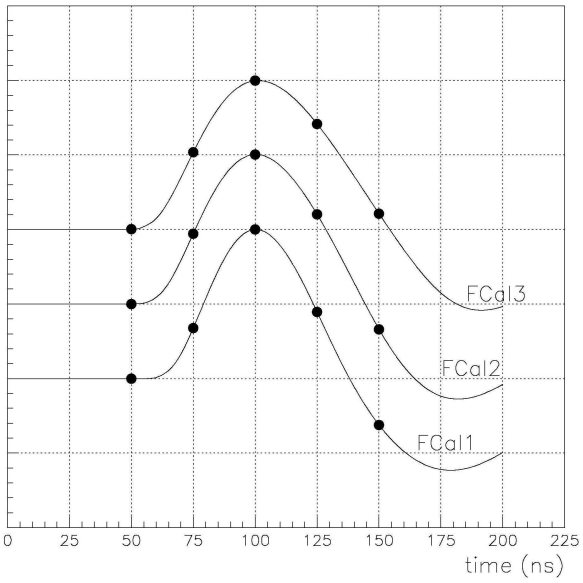

Figure 21. The pulse at the shaper output is bipolar. The shapes for each FCal module are different because of the different drift times at the electrodes and the different ganged electrode capacitances. Superimposed on each pulse are the pulse samples taken by the pipeline and digitized by the ADCs.

On the Front-End Board the signal first goes to a preamplifier [37] which, to a good approximation, preserves the signal shape and converts the current pulse to a voltage pulse by a factor (transimpedance) of about 890 Ω chosen to give the required dynamic range. The electronically cooled [38] input impedance of the preamp is about 25 Ω to match the pigtail impedance, thereby preventing reflections.

The signal then enters a CR-RC^2 (one differentiation and two integration stages) shaper [39] with characteristic time of each stage of about 13 ns. Figure 21 shows the bipolar pulse out of the shaper. Because the triangle pulse on the electrodes is so short, the negative lobe of the shaper pulse is an unusually large fraction of the peak of the positive lobe. The shaper has three separate gains, each roughly a factor 10 higher than the preceding one. For the high gain, the peak of the output pulse for a step function input is amplified by a factor of about 81.

Four shaper channels (each with the three gains) occupy one chip. Including the triangle pulse, the ZC_D integration, and the shaper, the overall transfer function peaks at a frequency of about 4 MHz.

Each of the three gains from a shaper channel then go to an analog pipeline [40]. This pipeline samples the shaper pulse at 25 ns intervals with a phase such that the third sample falls, on average, at the peak of the pulse. The pipeline runs continuously and is 128 samples deep in order to store the pulse while the Level 1 trigger makes a decision. The level 1 trigger latency is about 2.0 μs, short enough to capture the pulse before it falls off the end of the pipeline. When the Level 1 trigger decides to read out a particular event, the pipeline output is multiplexed to 12-bit ADCs with pedestal set at about 1000 counts. Digital threshold logic on the Front End Board looks at the third time-sample to decide which gain (of three) to read out. While up to 32 samples can be read out, the standard during routine data-taking is 5 samples.

The thresholds for switching gains are set so that the peak of the positive lobe doesn't overflow the ADC. With a pedestal at about 1000 counts, this leaves a range of less than 3095 counts. But when reading out more than 5 time samples, the negative lobe will underflow well before the positive lobe overflows so the gain-switching thresholds must be re-adjusted.

In addition to the four shaper channels, the shaper chip also contains a linear mixer, with a programmable choice of two output gains and a separate shaping circuit. This mixer adds the four channels together for the Level 1 trigger. The linear mixer output of the shaper chips are sent to Layer Sum Boards [41], two per Front End Board. These are customized mezzanine cards where weighted analog sums are formed to allow vector E_T summing in the Level 1 trigger. These analog sums are next sent off the Front End Board to one of two Tower Driver Boards in the FCal Front End Crate. The Tower Driver Boards simply drive these analog trigger sums on long cables from the Front End Crate to a Level 1 Interface in the counting room.

The warm electronics is remarkably consistent from one channel to the next. Gain variations are about 2%. A precision calibration system monitors these gains and any variation with time. The Calibration Pulser Board [42] is used by all of the liquid argon calorimeters in ATLAS. It puts out a current pulse with a sharp rise time and an exponentially falling tail with an initial slope matched to the fall time of the triangle pulse. For the FCal this time was adjusted to be about 72 ns (a compromise between the different fall times of the three FCal modules) by selection of the inductor at the output stage. The Calibration Pulser Board has 128 channels.

For the other liquid argon calorimeters in ATLAS the calibration pulse is routed to the electrode. But for the FCal, the radiation is so severe that it was decided to route the signal instead to the Front End Board inputs. This is done via special printed circuit boards mounted behind the FEC base plane. One Calibration Pulser Channel is routed to one channel on each of the 14 FEBs in the FEC. A 681 Ω resistor couples the signal to the FEB input pin. All 14 inputs in parallel match the approximately 50 Ω output impedance of the Calibration Pulser channel.

Half the calibration pulse travels to the preamp on the FEB, the other half travels down the pigtail and reflects off the electrodes. That reflection comes sufficiently later that it is partially separated from the direct pulse. The direct pulse is used to calibrate the warm electronics while the reflected pulse is used to diagnose the cold electronics [43].

Those parts of the electronics chain which are unique to the FCal are the electrodes, the interconnects, and the summing boards. The length of the cold cable harnesses and the length of the pigtails were chosen specifically for the FCal but the cables and connectors are common with the accordion liquid argon calorimeters. The feedthrough and all of the warm electronics are in common with the accordion liquid argon calorimeters with the exception of the Layer Sum Boards and the special features on the back plane of the Front End Crate and on the Calibration Pulser Board.

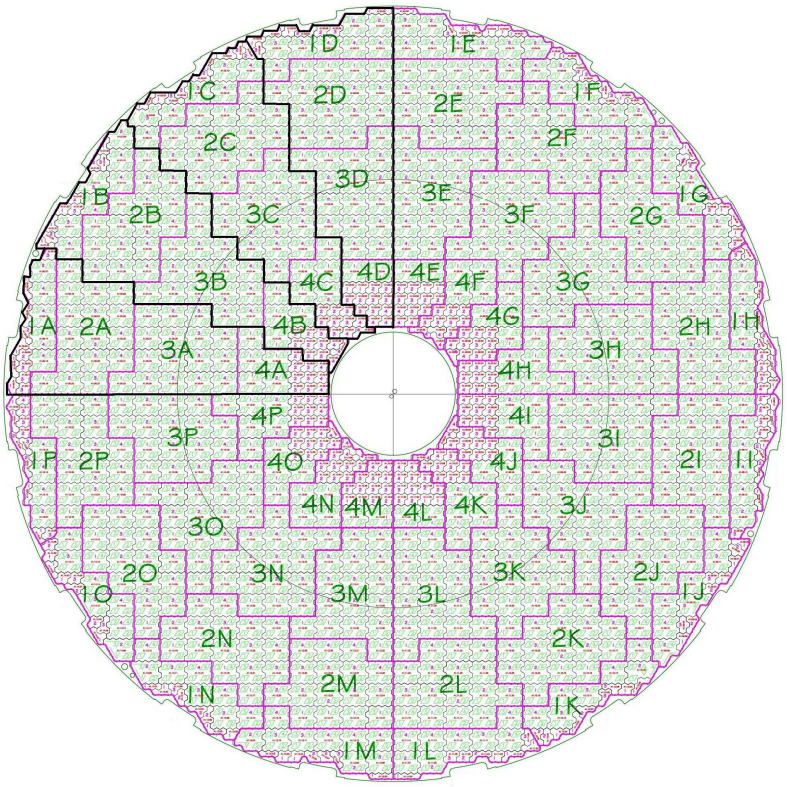

Figure 22. Front face of the FCal1A module. The η-φ bin trigger proto-towers are the irregular shapes designated by a number and letter such as 4A. Four of the 16 φ-slices are outlined in black for emphasis. Positive x is to the left in this view from the IP.

6. Noise

The bulk of the electronics noise is generated in the preamp. The coherent component in a readout channel is less than 5%. The electronics noise, predicted from measurements of the preamp and an understanding of the electronics chain, agrees with the measured value of 5.2 ADC counts on the high gain scale.

Measured in p_T, the rms pileup noise falls off slowly as |η| increases across the FCal. But the rms pileup energy increases such that the rms pileup noise dominates the electronics noise at $\mathcal{L} = 10^{34}$ cm^{-2} s^{-1}. The shaper pulse with a peaking time of about 40 ns leads to an rms pileup noise which, for the three FCal modules, in order, is about 19%, 36%, and 45% larger than the irreducible pileup noise from an ideal detector which has an integration time of one bunch crossing ("Pileup Penalty" in table 8). Tails on the pileup fluctuations are smaller than for liquid argon sampling calorimeters with longer drift times.

7. Segmentation

The hexagonal pattern of tube electrodes does not easily map onto the η-φ geometry appropriate to a detector at a hadron collider. An example of the approximate scheme we have adopted can be seen in figure 22and figure 23. The smallest segmentation level, the unit cell (see figure 9), is shown in figure 23. Each small circle represents the liquid argon gap in the unit cell. Parts of the hexagonal boundary of those unit cells on the boundary of a readout tile can be seen. The next segmentation level is the ganging of 4, 6, or 9 unit cells (for FCal1, FCal2, or FCal3) via the

2008 JINST 3 P02010

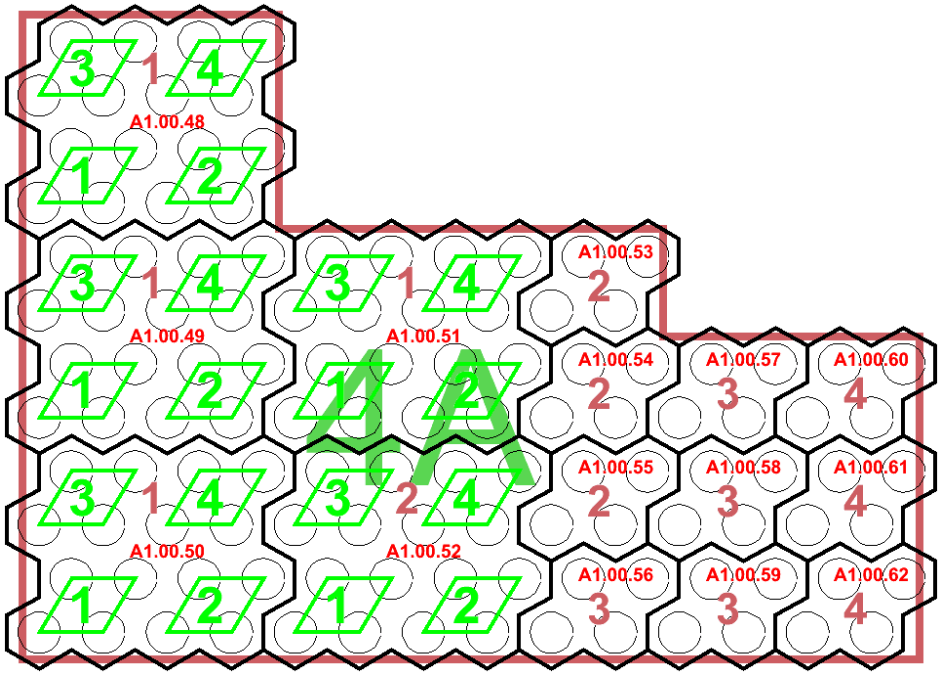

Figure 23. Details of the segmentation for the FCal1 module for one trigger proto-tower (4A) shown left of center in figure 22. The unit cells are shown with circles representing the liquid argon gap. The tube groups are groups of four electrodes. The readout cells are bounded by black lines, and the shaper sum association by numbers 1 through 4 located at the centers of the readout cells.

interconnect board to form a "tube group". Over most of the face of each module these tube groups are summed, via the transmission line transformers on the summing boards, into readout tiles. Near the inner and outer periphery of each module are tube groups which are not summed. These become readout tiles as they pass directly through the summing board. The signals from these readout tiles appear in the ATLAS data stream [44].

The face of each module is divided into 16 φ-slices and each φ-slice is divided into 4 η-bins. The boundaries of these η-φ bins respect the tube groups and readout tiles. The cables from the tube groups are organized into the cable harnesses by η-φ bins. The harnesses were produced with 64 cables each. For FCal1 there is one cable harness for each η-φ bin, for FCal2 there are two η-φ bins in the same φ-slice for each cable harness, and for FCal3 there is a full φ-slice for each cable harness. There are cases where one or two cables in a harness are not used because there are fewer than 64 tube groups in the assigned η-φ bin(s).

In the trigger path, four-fold sums are formed, without weighting, in the quad shaper chips. In figure 23 the four readout tiles labeled with a red "1" are summed in one shaper chip. Those labeled "2" in another shaper chip and so on to "4". Note that only three inputs to shaper chip "4" are used.

These η-φ bins are trigger proto-towers. These proto-towers are later summed in depth from module-to-module into trigger towers after being digitized at the input to the Level 1 Trigger. Drawings for all of the FCal modules can be found in reference [45].

2008 JINST 3 P02010

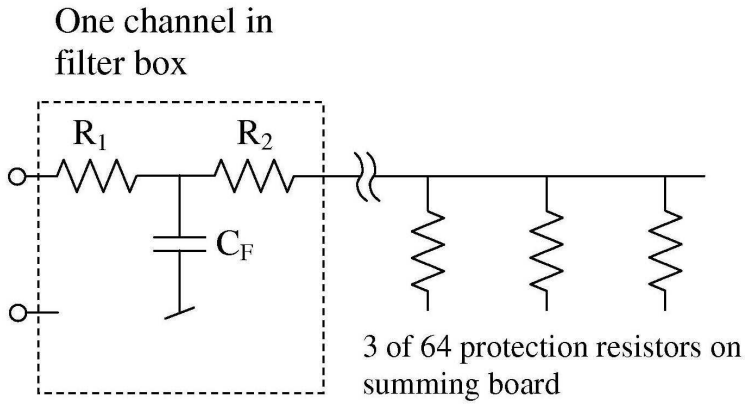

Figure 24. Schematic of one channel of the HV Distribution system. One HV supply channel connects at the left. The filter box on the HV feedthrough contains R_1 = 10 kΩ, R_2 = 1 kΩ, and C_F = 0.1 μF. Protection resistors are 1 or 2 MΩ. These same resistors are shown in figure 19.

8. HV distribution

The High Voltage system for the ATLAS Liquid Argon Calorimeters is based on ISEG supplies with a common control system [46]. The supplies for the FCal are of lower voltage (600 V max) and of higher current (6 mA max) than the norm. Lower values of these upper limits can be set both by screw-adjustment and/or in firmware. There are 8 HV channels on a PC board and two boards in one physical ISEG module. The voltage from the remote supplies is carried on long cables to the High Voltage feedthrough at the top rear of the endcap cryostat. The ground braid on each HV cable is connected at the ISEG supply but not at the feedthrough. The ground return current from the ISEG supply is carried by the signal grounds. This arrangement of the grounds is to avoid ground loops [47]. A total of 112 channels at each end is devoted to the FCal. The voltage is filtered at the feedthrough as shown in figure 24. The filter capacitor is grounded to the cryostat where the signals are also grounded. From the filter box the voltage is carried to a "warm" feedthrough (i.e. above the liquid level) and then on long constantan wires to a summing board. Four HV channels feed one summing board. There the voltage is distributed through protection resistors to each of the readout cables which feed each tube group. A few protection resistors are indicated in figure 24 and in figure 19. The summing board distributes the HV from each one of the four channels in a pattern which avoids adjacent tube groups. This way, if a HV channel should fail for some reason, no large, contiguous volume of an FCal module will be affected. Each readout tile will have at most one of four tube groups disabled by the loss of one HV channel.

9. Final assembly

The individual modules were constructed at the home institutions and then shipped to a clean room at CERN. During shipping each module was supported by a cradle which was encased within a steel framework. The module was constrained by a mandrel which fitted snugly into the beam hole in the module and was fixed at each end to the steel framework (figure 25). A foam-lined wooden crate was then built around this.

2008 JINST 3 P02010

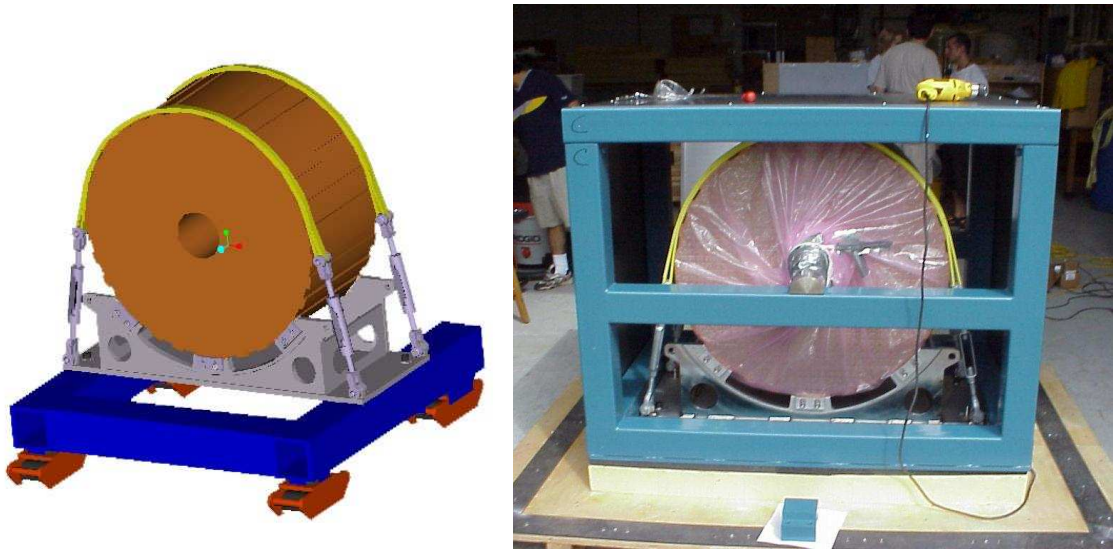

Figure 25. Schematic of shipping tooling (left) and photograph of one of the FCal3 modules ready for crating (right). The module cradle was also used during electrical testing at CERN and in the final assembly process.

Each module was subjected to a battery of electrical tests upon arrival at CERN, except for FCal3A which, for logistical reasons, was tested, cabled, and tested again just before shipment. Each electrode was tested to see that it held high voltage in air. Then the capacitance of each electrode was measured, as described earlier. The readout cable harnesses with interconnects on the ends were connected to the pins on the electrodes. Additional tests for high voltage breakdown were conducted and Time Domain Reflectometry data recorded. The latter test would find any cases where a cable ground was broken. DC tests would have missed this because all grounds are joined at the far end of the cable harness. Also capacitance measurements of the tube groups with cables were recorded.

In ATLAS each of the two end cap cryostats contains an Electromagnetic Endcap Calorimeter (EMEC), an Hadronic End Cap calorimeter (HEC), and an FCal as shown in figure 1. The LHC accelerator beam pipe must pass along the axis of the cryostat. The cryostat consists of an inner 'cold' vessel and an outer 'warm' vessel with vacuum in between. The inner cold vessel is subjected to large pressures. A structural member was added inside the cryostat to hold the cold vessel together along its axis. It was configured so that it could support the FCal as well. From the rear of the cryostat up to the front of the FCal this structural member is called the 'FCal support tube' [48]. The FCal sits snugly within this tube. See figures 2, 7, 26, 27 and 28. The thickness of the walls of this tube were specified to hold the cryostat together under forces up to about 200 tonnes. It also holds the weight of the FCal. Because the support tube is within the cold walls of the cryostat, there are holes in the wall of this tube to allow liquid argon to circulate. Each hole is fitted with a filter to trap any debris. From the front of the FCal to the front of the cryostat the structural member is conical, roughly projective to the IP. This conical section, called the 'forward cone' [49], also forms a part of the cold wall of the cryostat.

Radiation background simulations [50] indicated that the forward muon chambers, particularly the cathode strip chambers (CSCs), would suffer high background rates without additional shielding. For this reason a Plug3 was built of solid leaded red brass (alloy C83600, 85% Cu, 5% Sn, 5% Pb, 5% Zn) of outside dimensions nearly identical to the FCal modules [51] (table 3). The inner bore for the accelerator beam was stepped in radius with the same step

2008 JINST 3 P02010

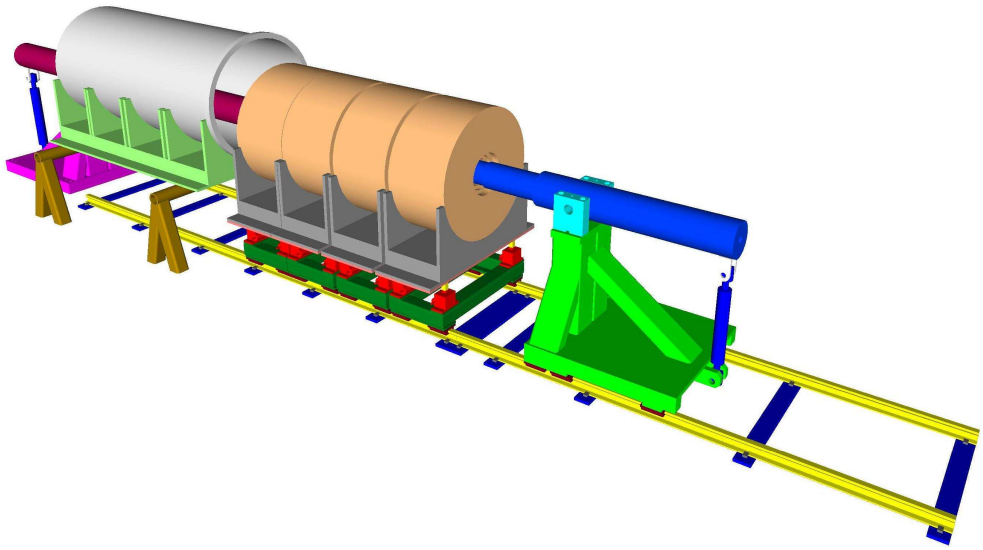

Figure 26. Final Assembly tooling. From left to right are the mandrel extension, the mandrel extension support, the FCal support tube, its cradle, its temporary frame, the rails, FCal1 on its cradle and cart, FCal2 on its cradle and cart, FCal3 on its cradle and cart, plug3 on its cradle and cart, the mandrel, and the mandrel support.

size as the modules. The Plug3 sits behind FCal3 and in front of the rear bulkhead of the cryostat. All of the FCal cables pass by Plug3 so it also has cable troughs around its outer periphery. In the front face of Plug3, a cavity had been cast to hold one of two argon purity monitors in each FCal assembly.

The final-assembly of each of the two ATLAS FCals consisted of aligning the three modules and the Plug3 on a mandrel, dressing the cables in their respective cable troughs, sliding the FCal support tube over the modules, bolting on the forward cone, with its inner cold tube, and bolting the rear bulkhead in place. The tooling for this procedure is shown in figure 26. It is based on a set of carts that ran on precision rails bolted to the floor. The carts were used to support the FCal modules and the Plug3 sitting on the same cradles used for shipping. Jacks under the cradles allowed for vertical alignment. Horizontal threaded pusher rods mounted on the carts allowed for transverse alignment. The other major component of the final assembly tooling was the final-assembly mandrel that consisted of a long, thick walled, hollow tube, stepped in diameter along its length, whose function was to support the modules and Plug3 in position at a critical point in the final-assembly process. The steps in the mandrel diameter were matched to the increasing inner diameters of each of the modules and Plug3. The mandrel was supported at one end by a framework which slid on the rails and which had a turn-buckle to hold its own weight in a cantilevered manner. At the other end of the mandrel a mandrel-extension was affixed and this was supported by a framework bolted to the floor at the end of the rails. The mandrel-extension was also a long, thick-walled tube whose ID fit snugly over the OD of the unsupported end of the mandrel. When bolted in place, the mandrel extension together with the mandrel spanned a distance of 4.55 m between supports. On top of the mandrel at positions where the modules would sit, adjustable shoes were located. The height of these shoes was adjusted to compensate for the anticipated sag of the mandrel and its extension under the load of the modules and Plug3. These shoes could be adjusted from the end of the mandrel via long, threaded rods located inside the inner bore of the mandrel. This was needed to account for the difference between the predicted and actual sag of the loaded mandrel.

2008 JINST 3 P02010

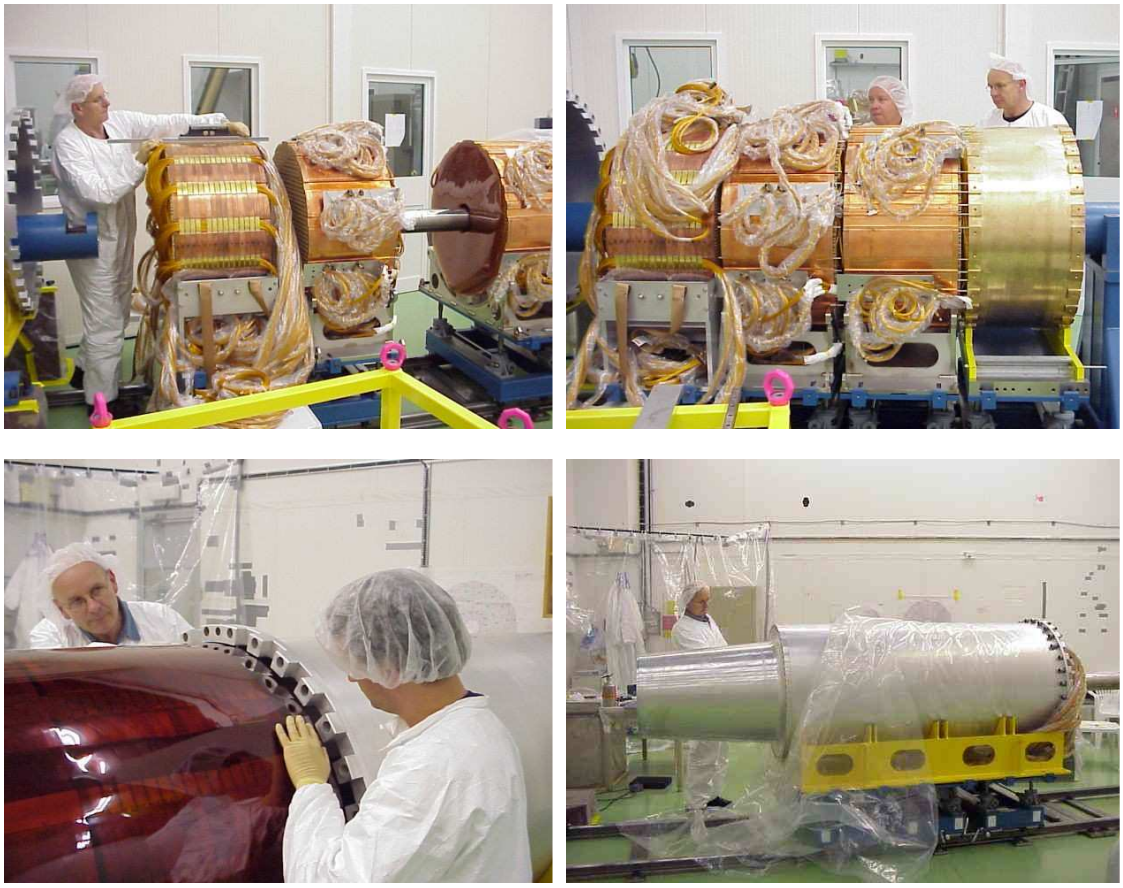

Figure 27. Upper-left: FCal1, FCal2, and FCal3 modules, from left to right, sitting on adjustable carts at the beginning of the alignment process. Part of the mandrel is visible between FCal2 and FCal3. Some of the readout coaxial cables are dressed into their cable troughs. Other cables are still in their protective plastic wrapping. The end of the cryostat support tube and mandrel extension can be seen at the extreme left. Upper-right: FCal1, FCal2, FCal3 and Plug3 are aligned on their carts ready for the cable harnesses to be dressed into their cable troughs. Lower-left: The FCal support tube is being moved over the modules. The polyimide sheet for electrical isolation wraps around the modules. Lower-right. The completed FCal assembly awaits installation of the rear bulkhead.

The final assembly procedure involved a number of alignment and displacement steps of the modules and the FCal support tube components. In the first part of the procedure the modules and Plug3 were aligned on their carts with the mandrel inserted through their beam holes (figure 27). With the cryostat support tube and its own cradle sitting on a temporary frame above the rails ahead of the modules, the mandrel-extension, threaded through this support tube, was affixed to the mandrel and bolted to it (figure 27). The jacks on the carts were lowered until the weight of the modules and Plug3 was carried by the mandrel. Minor alignment adjustments brought the modules and Plug3 into position. The carts were then moved forward to replace the temporary frame holding the cryostat support tube.

At this point the readout cable harnesses, the temperature probe readout cables, and four cables for each of two argon purity monitors were dressed into the cable troughs along the sides of the modules. Trough covers were screwed into place to constrain the cables within the troughs. The remaining lengths of the cable harnesses were suspended out of the way beyond the mandrel support. The modules were wrapped in polyimide sheet to electrically isolate the

2008 JINST 3 P02010

DC ground of the modules from the DC ground of the cryostat. Polyimide sheet was also positioned between modules for further electrical isolation.

After aligning the support tube on the carts, the support tube was moved over the modules and Plug 3 (figure 27). The radial clearance at room temperature between the OD of the modules and the ID of the cryostat support tube is about 2 mm. Via the jacks on the carts, the cryostat support tube was raised by the amount of the mandrel sag plus about 1 mm to take the weight of the modules and Plug3, now held inside the cryostat support tube. At this time the mandrel-extension was removed and the mandrel withdrawn from within the module beam holes.

The forward cone section was next bolted to the front of the cryostat support tube (figure 27). As the cone was moved into position, an argon purity monitor was inserted into a small cavity in the flange of the cone and connected to its cables which were already dressed into one of the cable troughs. The cold tube, which fits snugly within the module beam holes, had already been welded to the flange of this cone.

The cable harnesses were then arranged between the crenellations at the end of the support tube and the rear cold bulkhead was bolted into place.

10. Integration of the FCals into the cryostats

After the EMEC and HEC were inserted into the cryostat, the FCal summing boards were mounted on a framework on the rear face of the HEC. The pigtails from the feedthrough were connected to the summing board outputs and electrical tests from the feedthrough verified the connections. Time Domain Reflectometry allowed us to spot any signal or ground discontinuities and HV tests checked for any shorts. We also sent signals down the HV lines to check for any open circuits.

The cold cover was then mounted on the inner cryostat vessel. This cold cover has a concentric hole large enough for the FCal support tube to fit through and mating holes to accept the FCal rear cold bulkhead. The clearance between the outer radius of the support tube and the inner radius of the HEC is 12 mm. This close tolerance required that the FCal be introduced into the cryostat with great care. Extensive tooling had been fabricated for this procedure. The so-called “T2 tooling” consisted of a fixture which mounted on the rear of the FCal bulkhead. Another mandrel through the modules and Plug3 was attached to the rear bulkhead fixture and extended a short distance beyond the front of FCal1. A much larger diameter tube (the “T2 tube”) connected to this mandrel and fitted snugly within the front end of the forward cone (with a bearing ring to protect the cone from damage). The rear bulkhead fixture, the mandrel, and the T2 tube were designed so that the full weight of the FCal within the support tube, forward cone, and rear bulkhead could be supported from lifting points on the rear bulkhead fixture and the front of the T2 tube.

Some engineers worried that the stress analysis of this extreme loading did not account for the load points correctly. So a “sag” test was devised to verify the integrity of the scheme. With the FCal on its cradle, the T2 tube supported at its front end, and the rear bulkhead fixture supported from below, the jacks under the cradle were slowly lowered until the cradle no longer contacted the FCal. At this point the full weight of the FCal and its T2 tooling was carried as envisioned in the worst case loading. Under the load the FCal at the joint between the cone and support tube sank about 2 mm from the position it was in before the jacks were lowered. The upper left panel in figure 28 shows one step in preparations for this “sag” test.

2008 JINST 3 P02010

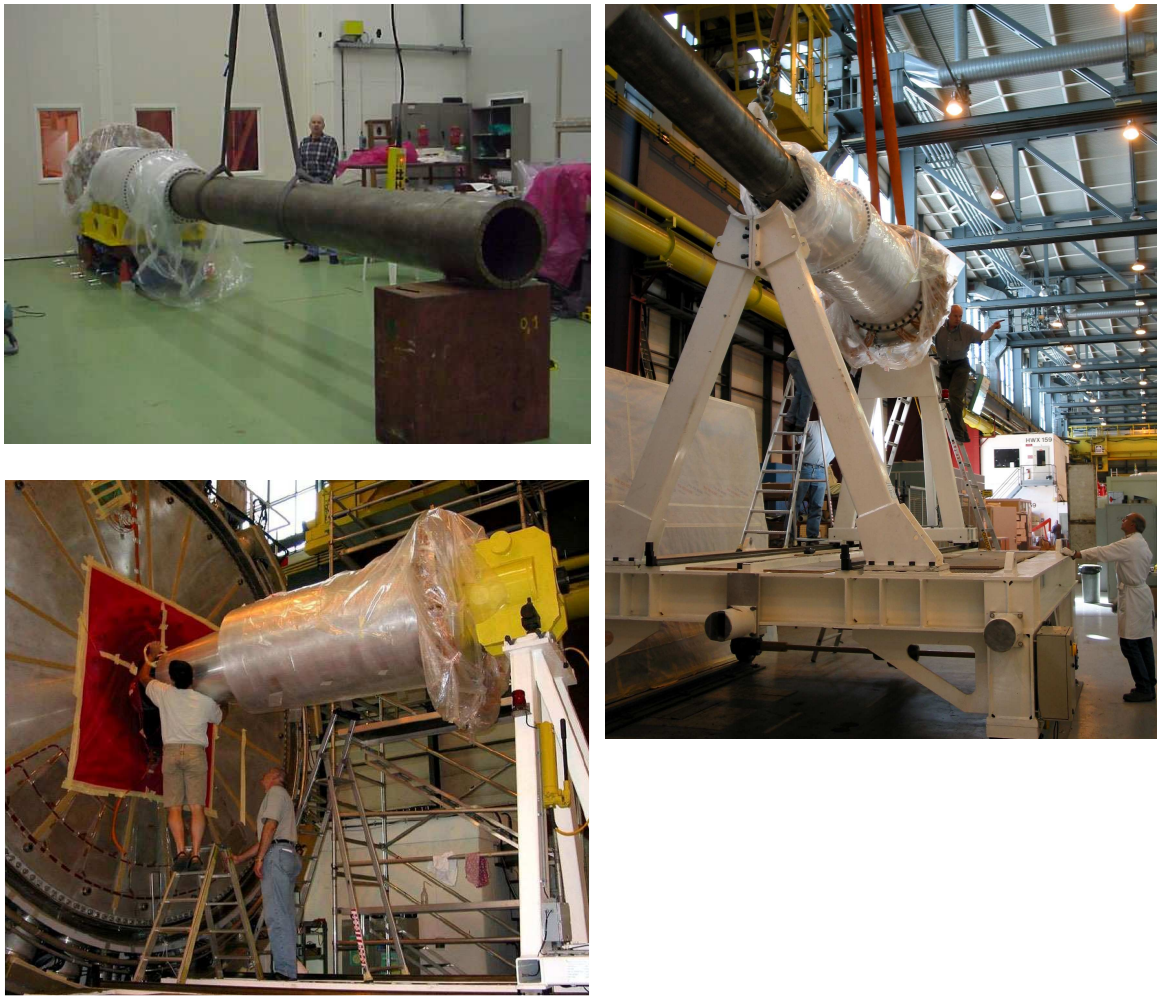

Figure 28. Upper left: FCal with T2 tube undergoing "sag" test. Upper right: FCal and T2 tube on T6 truck just downstream of the endcap cryostat. Lower left: The forward cone is just entering the cold vessel of the cryostat.

The FCal was then transported from its cleanroom to the staging area. With the rear bulkhead fixture, the mandrel, and the T2 tube, the FCal was placed on a large "truck" on rails. The photo in the upper right of figure 28 shows the FCal being lowered by crane onto this truck. The FCal was supported at the rear by the bulkhead fixture attached to a frame at the rear of the truck. At the front, the FCal was supported by the T2 tube resting on a frame at the front of the truck. Most of the T2 tube extended beyond the front of the truck.

At this point the truck was advanced towards the rear of the endcap cryostat. The rails were already aligned with the cryostat. The T2 tube advanced completely through the cryostat and, when it extended out of the front of the cryostat, its weight was held by rollers on another frame. The weight was transferred by removing the frame at the front of the truck. With this frame removed, the truck could be advanced the rest of the way as depicted in the lower left of figure 28.

When the rear FCal bulkhead was about 30 cm from mating with the cryostat cold wall, the advance was interrupted so that the FCal cable harnesses could be attached to the input connectors on the FCal Summing Boards. As connections were made, time domain

2008 JINST 3 P02010

reflectometry tests from the feedthrough confirmed the integrity of the contacts. The temperature probe wires and purity monitor cables were also connected.

The FCal was advanced the last 30 cm and the FCal rear bulkhead sealed and bolted to the cryostat cold wall. The T2 tooling was then removed. After problems with the seals on the cryostat cold vessel were solved, the parts of the warm wall in front of the FCal and along the beam line concentric with the FCal were put into place and sealed, bolted, and welded.

After the cryostat drawings [20] were produced it was decided to move the cryostats back by 40 mm. The position quoted in the caption of table 3 assumes this modification. As of this writing, the end cap cryostats are not in their final positions in the ATLAS cavern. Services for the inner tracker may force the cryostats to sit further from the IP than is currently intended.

11. Test beam performance

A series of beam tests was carried out to evaluate various aspects of the ATLAS Forward Calorimeter system, including tests of prototypes and of the three final FCal modules (FCal1, 2, and 3) which make up one of the two Forward Calorimeters. Recent testing was conducted in the H6 beam line in the North Area at CERN. This beam provided electrons and hadrons with momenta from 10 GeV/c to 200 GeV/c. The incident beam particles encountered 1) thin, plastic scintillation trigger and veto counters, 2) 1 mm wire spacing proportional chambers, and 3) a differential gas Cerenkov counter before hitting the Forward Calorimeter. Behind the cryostat containing the FCal modules were 1) an iron-plate/scintillator "tail-catcher" calorimeter, 2) an iron and concrete beam dump, and 3) a scintillator to tag muons. These beam line devices allowed us some beam-particle identification and allowed for rejection of multiple particles and particles which scattered somewhere upstream. Results of the prototype tests can be found in references [52]-[55]. The beam test of the three final FCalC modules was used to evaluate the performance of the final system and demonstrated that the FCal system meets the performance goals in terms of its energy resolution and the magnitude of the tails of the energy resolution function. The results and analyses are described in detail in reference [56]. Here we give a brief summary.

Summing all FCal1 calorimeter energy within a radius of 8 cm from the shower core we find an electron energy resolution of about

$$\frac{\Delta E}{E} = 3.5\% \oplus \frac{28.5\%\sqrt{\text{GeV}}}{\sqrt{E}}$$

with about 1.2 GeV rms of electronics noise added in quadrature. Summing all FCal1, 2, and 3 calorimeter energy within 16 cm of the shower core, we extract a pion energy resolution of about

$$\frac{\Delta E}{E} = 7.5\% \oplus \frac{94\%\sqrt{\text{GeV}}}{\sqrt{E}}$$

with about 5.3 GeV rms of electronics noise added in quadrature. From shower sharing in neighbor calorimeter channels, we can determine the impact position of the incident particle from the calorimeter alone and compare that with the position extrapolated via the beam proportional chambers. We find the impact position resolution for electrons to be of order 1 mm at energies above 100 GeV [53] and of order 2 mm for 200 GeV hadrons. A position determination allows a study of the response variation in the transverse direction due to the electrode structure. This produces a map of the response with a periodicity of the unit cell. Using this response map we have corrected the electron energy determination for impact

2008 JINST 3 P02010

position. The constant term in the energy resolution drops to about 2.5%. If the position determination were better this correction might have reduced the constant term even more.

In ATLAS the FCal will often be used to measure jets. In determining the jet energy we will sum over many particles. This energy summing will average over the impact position of the jet particles. Thus for jets with many particles the constant term in the energy resolution should decrease from the single particle value, approaching the sub-dominant contribution to the constant term which we presently estimate at about 2.5% for electrons.

Large tails on the energy resolution function can lead to a false missing E_T signal. For 200 GeV hadrons incident on the FCal we determine the probability that the FCal will measure the energy to be greater that 300 GeV as 2.4×10^{-4} and the probability that the FCal will measure the energy to be less than 100 GeV as 5.2×10^{-4}. Of the hadrons with measured energy below 100 GeV, about 90% were late showering hadrons with significant energy leakage out the back of the calorimeter. Half the remaining were muons.

The timing resolution for a single channel near the center of the beam spot for 200 GeV electrons was measured to be about 250 ps relative to the test beam trigger from the timing scintillator in the 3-fold coincidence. Because all three scintillators were timed relative to each other by a TDC with 50 ps least count, the timing resolution of the trigger could be determined. When subtracted in quadrature the timing resolution of the FCal was found to be about 130 ps. But much of this remaining jitter comes from a timing component on the Front End Board so the intrinsic timing resolution of the FCal itself should be much better.

Our best estimates of 'e'/'mip' and 'e'/'π' are shown in table 8. In the table, the 'π' value for FCal3 is not biased by shower leakage. Different weights, particularly for FCal3, might be employed to correct for the small shower leakage out the back.

12. QA/QC

Electrical testing of the modules was done often during the detector assembly and cabling phases. All problems found in these tests were repaired. The cabled modules were cold tested in liquid nitrogen in the H1 cryostat in the CERN North Area before the final assembly stage. In the summer of 2003 a beam test of the three FCalC modules also served as a longer term test of the HV integrity. Electrical tests were done after installation of each FCal into the endcap cryostat, using a TDR system connected at the baseplane of the front end crate. These tests were performed during cold tests that took place on the surface and were repeated after warmup and transport of the endcap cryostats to the surface above the ATLAS cavern. After lowering the cryostats into the cavern and installing the front-end electronics, the ATLAS DAQ system was used to record the signals from calibration pulses. As described earlier, the reflected half of the calibration pulse allows us to detect calorimeter faults, such as shorted electrodes or damaged electrical components on the summing boards.

On the modules the most common defects are high-voltage shorts which prevent a tube group from holding voltage. A few shorts have appeared at points along some of the coaxial cables, probably pinched during final assembly. Another fatal defect can occur on the summing board due to a damaged blocking capacitor which prevents a tube group from being read out. Shorts and damaged blocking capacitors affect a single tube group, so a quarter of a readout channel in most cases, or a whole readout channel in the case of an un-summed channel. For summed channels the other three tube groups are functional, and techniques are being developed to help correct for the lost tube group.

2008 JINST 3 P02010

Module	Tube Groups			Channels		
	Dead	Distorted	Good	Dead	Distorted	Good
FCal1A	24	2	3040	0	26	982
FCal2A	7	1	1692	1	4	495
FCal3A	62	0	852	1	59	194
FCal1C	50	1	3015	5	51	952
FCal2C	4	4	1692	0	8	492
FCal3C	5	0	909	1	4	249

Table 10. Faults found in commissioning data from the reflected calibration pulse.

A number of tube groups developed faults in the FCal installation phase after the completed FCal was inserted into the endcap cryostat. In addition, two of the 224 HV lines which serve the FCals were lost, one in FCalC and one in FCalA. A lost HV line results in a loss of a quarter of the tube groups in the region of φ served by the summing board, but as noted earlier these tube groups are not contiguous.

Table 10 shows the known faults in the FCal modules installed in the ATLAS cavern as derived from analysis of commissioning data. These were derived from the data taken in special calibration pulser runs reading out 32 samples in order to see the reflected pulse from the FCal electrodes.

13. Materials certification

All the FCal materials going into the cryostat were subjected to a certification program which tested for integrity under a neutron fluence comparable to a year of running at nominal luminosity at the LHC and at the worst location in the FCal [57]. There was also a material test with an exposure of about 10 MRad of ionizing radiation. The equivalent exposure should have been longer but this was all that the facility could manage. The materials were exposed to a beam of fast neutrons from a pulsed neutron reactor for about 11 days while inside a liquid argon cryostat. The purity of the argon was measured before and after the irradiation. There was a slight hint that the purity improved after irradiation but the difference was within the small uncertainty of the measurement. Materials tested included the PEEK fiber, the coax cable with polyimide dielectric and insulation, and the interconnect boards. In a separate exposure, which included a piece of the PC board, connectors, protection resistors, blocking capacitors, and transformers, the summing board components received the same treatment.

14. Summary

ATLAS has elected to locate the forward calorimeters at about the same distance from the IP as the endcap calorimeters despite the severe radiation environment in order to realize several benefits. The modules are liquid argon, ionization, sampling calorimeters with novel liquid argon electrode structures and are particularly dense to minimize the longitudinal and transverse shower spreading. Proximity to the neighboring Hadronic Endcap Calorimeter minimizes energy mismeasurements due to spray and dead material between the two. Space charge effects, beam heating, and radiation damage considerations shaped the design of the calorimeters. The three FCal modules at each end of ATLAS were constructed at the home institutions and

2008 JINST 3 P02010

shipped to CERN where they were packaged into the two FCal assemblies. They were installed into the endcap cryostats on schedule. Test beam results with electrons and hadrons show performance exceeding the requirements. Commissioning data show a tolerable level of failures and problem channels.

Acknowledgments

We would like to thank the rest of the liquid argon group within the ATLAS collaboration for help, advice, good ideas, and support during all phases of the construction project. We would also like to thank Teresa Embry, Keith Coley, and Philippe Gravelle who made major contributions to the construction and assembly of the FCal detectors. The following people have helped with various phases of the project: Michael Starr, Ken Green, Ted Moreno, Max Shkarayev, Peter Truncale, Robert Walker, Walter Lampl, Lullen Pajor, Brandon Cob, Charissa Fuhrmann, Joshua Ruder, John Hector, Kami Torrey, Jeremiah Weiner, Igor Koruga, Kim Whitley, Lik Hang Lee, Elizabeth Inrig, Robert Mahon, Witono Lukman, Aidarus Farah, Eustorgio Tesendiz-Hernandes, Michal Samborski, Rebecca Oommen, Tao Yu, Muzammil Mehdi, V. Serezhin (deceased), S. Zel'dovich, Rob Ashby, Akos Bakos, Ryan Bolan, Doug Christie, Denise Cooper, Mei Lee Fong, Metin Guler, Carmen Higgins, Alexander Hudek, Asif Hussain, Samir Iskander, Marcus Kaevats, George Makram, Greg Mohammed, Harold Solomons, Shakila Satar, William Sunday, Paul Toth, and Shariar Zayyani. This work was funded by the Natural Science and Engineering Research Council of Canada, the US Department of Energy, the Russian Federal Agency for Atomic Energy and the RF Ministry of Education and Science, and the NSF and MOST of China.

References

[1] The ATLAS collaboration, *Technical Proposal for a General-Purpose pp Experiment at the Large Hadron Collider at CERN*, CERN/LHCC/94-43 (1994).

[2] PARTICLE DATA GROUP collaboration, W.-M. Yao et al., *Review of Particle Physics*, *J. Phys.* **G 33** (2006) 1.

[3] J. Rutherfoord, *Heating and cooling a forward calorimeter*, ATLAS Note ATL-CAL-94-056, Geneva, CERN (1994).

[4] ATLAS collaboration, *ATLAS letter of intent for a general-purpose pp experiment at the Large Hadron Collider*, CERN/LHCC/92-4 (1992).

[5] J. Rutherfoord, L. Shaver and M. Shupe, *The ATLAS Forward Region*, ATLAS Note ATL-CAL-94-035, Geneva, CERN (1994).

[6] M. Shupe and J. Rutherfoord, *Three Options for the ATLAS Forward Region: Particle and Jet Response and Fluence Results from a GEANT Mixture Description of the Detector*, ATLAS Note ATL-CAL-94-036, Geneva, CERN (1994);
M. Shupe, *Using GEANT Mixtures for the Precise Simulation of Particle and Jet Response, and Particle Fluxes in ATLAS*, ATLAS Note ATL-CAL-94-037, Geneva, CERN (1994).

[7] J. Rutherfoord, A. Savin, L. Shaver and M. Shupe, *The ATLAS Integrated Forward Calorimeter, Progress on Answers to Calorimetry Panel Questions*, ATLAS Note ATL-CAL-94-055, Geneva, CERN (1994).

2008 JINST 3 P02010

[8] L. Waters and W.B. Wilson, *LAHET/MCNP/CINDER'90 Activation Calculations for the ATLAS Integrated Forward Calorimeter Concept*, ATLAS Note ATL-CAL-94-047, Geneva, CERN (1994).

[9] J. Dowell et al., *Report of the ATLAS Review Panel on Forward Calorimetry*, ATLAS Note ATL-GEN-94-007, Geneva, CERN (1994).

[10] A. Artamonov, *Calorimetry Performance in the Forward Region*, ATLAS Note ATL-CAL-94-065, Geneva, CERN (1994).

[11] M. Shupe, *ATLAS Muon Region Background Fluxes in Four Forward Configurations*, ATLAS Note ATL-GEN-94-011, Geneva, CERN (1994).

[12] G. Battistoni, A. Ferrari and P.R. Sala, *Background calculations for the ATLAS detector and hall*, ATLAS Note, ATL-GEN-94-010, Geneva, CERN (1994).

[13] ATLAS collaboration, *ATLAS Liquid Argon Calorimeter Technical Design Report*, CERN/LHCC/96-41, ATLAS TDR 2 (1996).

[14] D. Gingrich et al., *Construction, assembly and testing of the ATLAS hadronic end-cap calorimeter*, (2007) *JINST* **2** P05005.

[15] J. Rutherfoord, *Ion Loading in Liquid Ionization Calorimeters*, GEM TN-91-27 (1991); *Testing for Effects of Ion Loading in Liquid Ionization Calorimeters*, GEM TN-93-410 (1993); *Signal degradation due to charge buildup in noble liquid ionization calorimeters*, *Nucl. Instrum. Meth.* **A 482** (2002) 156.

[16] P. Loch, *Tube Radius Optimization for the Electromagnetic Forward Calorimeter in ATLAS*, ATLAS Note ATL-LARG-96-039, Geneva, CERN (1996).

[17] J. Rutherfoord, *The Shape of the ATLAS Forward Calorimeter Current Pulse*, ATLAS Note ATL-LARG-PUB-2006-004, Geneva, CERN (2006).

[18] G. Bélanger et al., *The ATLAS Liquid Argon Forward Calorimeter: Electrode Uniformity*, ATLAS Note ATL-LARG-PUB-2006-001, Geneva, CERN (2005).

[19] J. Rutherfoord, *Sensitivity of the Signal to the Gap*, ATLAS Note ATL-LARG-95-020, Geneva, CERN (1995).

[20] G. Mace drawing http://edms.cern.ch atlaec_0004-vAB.plt.

[21] G. Bachy, *Co-ordinate Axis Systems*, ATL-GE-QA-2041 (1996).

[22] L. Shaver drawing http://edms.cern.ch atlaew_0006-v0.plt.

[23] For characteristics under radiation see H. Schoenbacher and A. Stolarz-Izycka, *Compilation of Radiation Damage Test Data*, CERN 79-04 (1979), and see table 2a which was added later.

[24] HeliCoil M6×1 Part No. 5403-6, Emhart Fastening Teknologies, Industrial Division, Shelton, CT 06484 USA, http://www.emhart.com/products/helicoil.asp.

[25] Mill-Max Mfg. Corp., Oyster Bay, NY 11771 USA, http://www.mill-max.com Part Number 5601-0-01-15-00-00-03-0.

[26] Mill-Max Mfg. Corp., Oyster Bay, NY 11771 USA, http://www.mill-max.com Part Number 0285-0-15-15-16-14-10-0.

2008 JINST 3 P02010

[27] Autosplice Inc., San Diego, CA USA, http://www.autosplice.com Part Number: 8-25920591324BB.

[28] Mill-Max Mfg. Corp., Oyster Bay, NY 11771 USA, http://www.mill-max.com Custom Part Number 9211-0-00-15-00-00-33-0.

[29] Mill-Max Mfg. Corp., Oyster Bay, NY 11771 USA, http://www.mill-max.com Custom Part Number 9213-0-00-15-00-00-33-0.

[30] Mill-Max Mfg. Corp., Oyster Bay, NY 11771 USA, http://www.mill-max.com Custom Part Number 4117-0-15-15-34-14-40-0.

[31] J. Rutherfoord, *Electrode Transmission Line Corrections to the ATLAS Forward Calorimeter Pulse*, ATLAS Note ATL-LARG-PUB-2006-005, Geneva, CERN (2006).

[32] Ohmite Mfg. Co., Rolling Meadows, IL 60008 USA, www.ohmite.com. The 1 MΩ resistors are P/N MC101821004F while the 2 MΩ resistors are P/N MC101822004F.

[33] Johanson Dielectrics, Sylmar, CA 91342 USA, www.johansondielectrics.com. The capacitors rated at 500 V are P/N 501H51N123JY4E while those rated at 1000 V are P/N 102H66N123KY4E.

[34] C.L. Ruthroff, *Some Broad-Band Transformers*, *Proc. I.R.E.* **47** (1959) 1337;
S. Tansal and H. Sobol, *Wide-Band Pulse Transformers for Matching Low Impedance Loads*, *Rev. Sci. Instrum.* **34** (1963) 1075.

[35] MWS Wire Industries, Westlake Village, CA 91362 USA, http://www.mwswire.com/twistite1.htm Twistite P/N T-4281289-10.

[36] C. Collard, D. Fournier, S. Henrot-Versille and L. Serin, *Prediction of signal amplitude and shape for the ATLAS electromagnetic calorimeter*, ATLAS Note CERN-ATL-COM-LARG-2007-009; Measurements at Brookhaven National Lab yield impedance values in the range 36 to 37 Ω; F. Lanni, BNL, private communication.

[37] R.L. Chase, C.de La Taille, S. Rescia and N.Sequin, *Transmission line connections between detector and frontend electronics in liquid argon calorimetry*, *Nucl. Instrum. Meth.* **A 330** (1993) 228; R.L. Chase and S. Rescia, *A linear low power remote preamplifier for the ATLAS liquid argon EM calorimeter*, *IEEE Trans. Nucl. Sci.* **44** (1997) 1028.

[38] V. Radeka, *Signal, noise, and resolution in position-sensitive detectors*, *IEEE Trans. Nucl. Sci.* **21** (1974) 51.

[39] J. Collet et al., *The LAr Tri-Gain Shaper*, ATLAS Note ATL-LARG-98-092, Geneva, CERN (1998).

[40] D. Breton, V. Tocut, P. Borgeaud, E. Delagnes, J. Parsons and W. Sippach, *HAMAC, a rad-hard high dynamic range analog memory for ATLAS Calorimetry*, 6th Workshop on Electronics for LHC Experiments, LEB 2000, Cracow, Poland, 11 – 15 Sep 2000.

[41] W. Cleland, *Layer Sum Boards for the ATLAS Liquid Argon Calorimeters (PRR)*, ATLAS Engineering/Technical Note 2000-04-09, CERN ATL-AL-EN-0019.

[42] J. Colas et al., *The LArg calorimeter calibration board*, ATLAS Note ATL-LARG-2000-006, Geneva, CERN (1999);
N. Dumont-Dayot et al., *The ATLAS LAr Calibration board*, 9th Workshop on Electronics for LHC Experiments, LECC 2003, Amsterdam, The Netherlands, 29 Sep – 03 Oct 2003.

2008 JINST 3 P02010

[43] J. Rutherfoord and A. Savin, *ATLAS FCal Diagnostics using the Calibration Pulse*, ATLAS Note ATL-LARG-2004-010, Geneva, CERN (2004).

[44] A. Bazan et al., *ATLAS liquid argon calorimeter back end electronics*, 2007 *JINST* **2** P06002.

[45] Segmentation drawings by L. Shaver can be found at http://edms.cern.ch atlaew1_0001-vAB.plt, atlaew1_0008-v0.plt, atlaew2_0001-vAA.plt, atlaew2_0017-v0.plt, atlaew3_0001-vAB.plt and atlaew3_0016-v0.plt.

[46] http://atlas.web.cern.ch/Atlas/GROUPS/LIQARGON/Electronics/Power_Cooling/HV_supplies/index.html

[47] V. Radeka, *Shielding and Grounding in Large Detectors*, Proc. 4th Workshop on Electronics for LHC Experiments, CERN/LHCC/98-36(1998).

[48] G. Mace drawing, http://edms.cern.ch atlaecc_0008-vAA[1].plt.

[49] G. Mace drawing, http://edms.cern.ch atlaecc_0007-vAA[1].plt.

[50] S. Baranov, M. Bosman, I. Dawson, V. Hedberg, A. Nisati and M.Shupe, *ATLAS Radiation Background Task Force Summary Document*, ATLAS Note CERN-ATL-GEN-2005-001, Geneva, CERN (2005).

[51] G. Mace, L. Shaver and B. Szeless, *Copper Shield Plug, Specification*, CERN ATL-AE-ES-0008 (2000);
L. Shaver drawing, atlaej3_0009-v0.plt.

[52] M.I. Ferguson et al., *Electron testbeam results for the ATLAS liquid argon forward calorimeter prototype*, *Nucl. Instrum. Meth.* **A 383** (1996) 399.

[53] A.Savine et al., *Position measurements and response uniformity of the LAr FCal*, Proc. VIIth Int. Conf. on Calorimetry in High Energy Physics, Tucson, 1997, E. Cheu, T. Embry, J. Rutherfoord and R. Wigmans eds., World Scientific, Singapore (1998).

[54] A. Savine, *Hadronic Energy Resolution Improvement in Calorimeter with Fine Transverse Segmentation*, Proc. IX Int. Conf. on Calorimetry in High Energy Physics, Annecy 2000, B. Aubert, J. Colas, P. Nedelec and L. Poggioli eds, Frascati Physics Series (2000).

[55] J. Armitage et al., *Electron Signals in the Forward Calorimeter Prototype for ATLAS*, 2007 *JINST* **2** P11001.

[56] J.-P. Archambault et al., *Energy Calibration of the ATLAS Liquid Argon Forward Calorimeter*, 2008 *JINST* **3** P02002.

[57] C. Leroy et al., *Liquid Argon Pollution Tests of the ATLAS Detector Materials at IBR-2 Reactor in Dubna*, *Part. Nuclei Lett.* **5** (2000) 102; *Radiation Hardness Tests of the ATLAS Liquid Argon Calorimeters Materials and Equipments at the IBR-2 Reactor in Dubna*, submitted to Nucl. Instrum. Methods, Sept. 2003; *Irradiation Tests of Readout Chain Components of the ATLAS Liquid Argon Calorimeters*, *Part. Nuclei Lett.* **5** (2000) 102; *Irradiation tests of ATLAS liquid argon forward calorimeter (FCAL) electronics components*, ATLAS Note ATL-LARG-2002-003, Geneva, CERN (2002).

2008 JINST 3 P02010